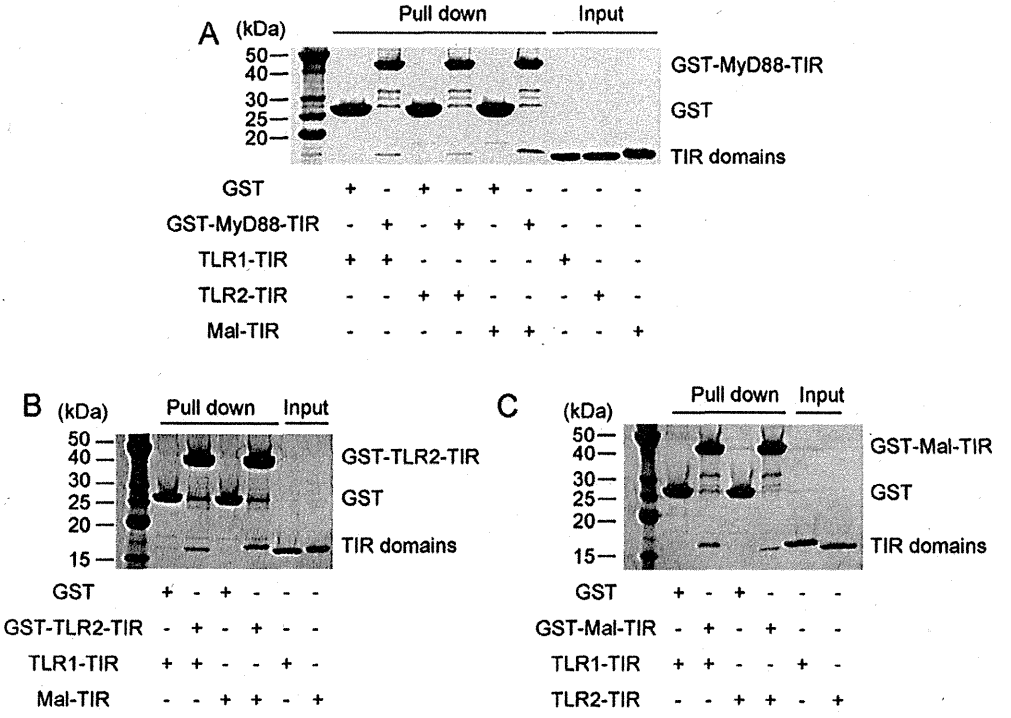

Fig. 2. Analysis of direct interactions between the TIR domains involved in TLR2 signaling using GST pull-down assays. (A) Binding assays for MyD88-TIR with TLR1-TIR, TLR2-TIR or Mal-TIR. GST-MyD88-TIR binds TLR1-TIR, TLR2-TIR and Mal-TIR. (B) Binding assay for TLR2-TIR with TLR1-TIR or Mal-TIR. GST-TLR2-TIR binds both TLR1-TIR and Mal-TIR. (C) Binding assay for Mal-TIR with TLR1-TIR or TLR2-TIR. GST-Mal-TIR binds both TLR1-TIR and TLR2-TIR.

an *E. coli* expression system (Materials and Methods). The 2D ^{1}H–^{15}N correlation spectra of the MyD88-TIR mutants showed widespread patterns in the backbone amide ^{1}H–^{15}N cross-peaks, which were mostly superimposable with that of the wild-type MyD88-TIR (Fig. 4A), indicating no substantial structural change was induced by the amino acid substitution. In the spectra of the Arg-196 and Arg-217 mutant proteins, and the Lys-282 and Arg-288 double mutant proteins, cross-peaks of F164, I165, C168, L191, V193, S194, G201, V204, S206, A208 and E210, cross-peaks of F161, D162, A163, K190, C192, S194, E213, G246, L289, S294 and L295, and cross-peaks of K256, Y257, F264, S266, R269, F270, I271, D275, T277, C280, T281, S283, F285, T287, L289 and K291 disappeared in the original positions of the MyD88-TIR wild-type, respectively (Ohnishi et al., 2010). However, in most cases, cross-peaks could be found very close to the original positions, which are presumably from the corresponding residues (Fig. 4A). In the spectrum of the R217A mutant, the G201 cross-peak does not appear; it exists at the same position as that of the wild-type but with lower intensity than the threshold used to generate the figure. These residues are mapped onto the structures of MyD88-TIR

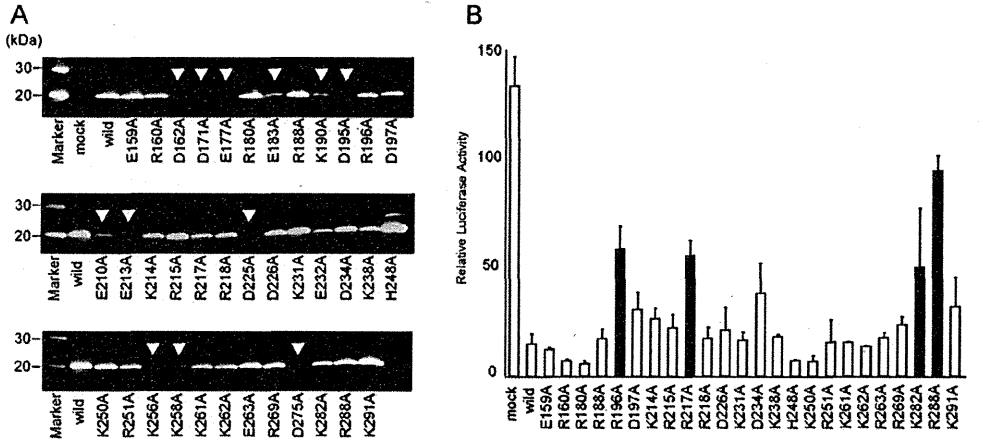

Fig. 3. Functional assay for MyD88-TIR in TLR1/TLR2 signaling. (A) Evaluation of the expression levels of all of the alanine-substituted mutant proteins containing MyD88-TIR in HEK293 cells. Arrowheads indicate mutants with poor expression levels. The expression levels of D162A, D171A, E177A, E183A, K190A, D195A, E210A, E213A, D225A, K256A, K258A and D275A were significantly lower than those of the other mutants. (B) NF-κB reporter gene assay with Pam3CSK4-induced (0.1 μg/ml) 293-hTLR1/2 cells. In this graph, each column indicates the relative luciferase activity of the stimulated cells over the non-stimulated cells. Data represent the mean + S.D. of triplicate wells. This experiment is representative of at least three independent experiments. Black bars indicate the significantly increased NF-κB activity, as compared with the wild-type group. The statistical significance of the differences in the luciferase activities between the wild-type and mutants was analyzed using Dunnett's multiple comparison test. Statistical significance was assumed to be $P < 0.05$.

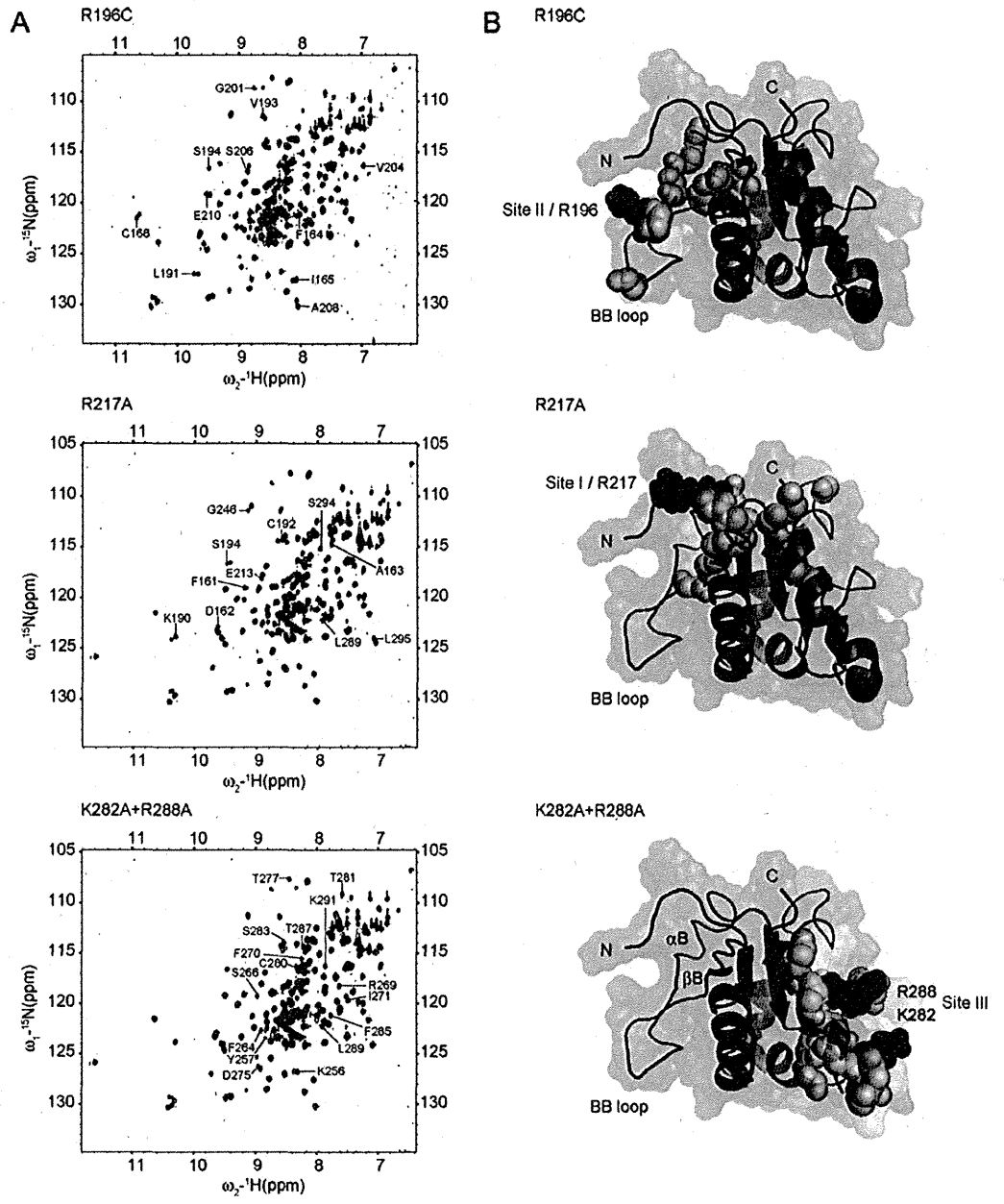

Fig. 4. ^{1}H–^{15}N correlation NMR spectra of MyD88-TIR. (A) Superimposition of ^{1}H–^{15}N correlation NMR spectra for the wild-type MyD88-TIR (red) and mutants (blue). The residues for which the cross-peaks disappeared in the original position of the wild-type MyD88-TIR in the 2D ^{1}H–^{15}N correlation spectra of the mutant proteins are indicated. (B) Structure of the MyD88-TIR (PDB ID: 2z5v) onto which Site I (Arg-217), II (Arg-196), III (Lys-282 and Arg-288) (red), and the residues for which the cross-peaks disappeared in the original position of the wild-type MyD88-TIR in the spectra of the mutant proteins (light brown) are mapped; these residues reside close to each mutated residues (Arg-196, Arg-217, Lys-282, or Arg-288). (For interpretation of the references to color in this figure legend, the reader is referred to the web version of this article.)

(Fig. 4B). The ribbon diagrams of MyD88-TIR structure were generated using the program PyMOL. Additionally, we also performed mutational analysis of MyD88 using a NF-κB luciferase reporter gene activity assay with HEK293T cells transfected with plasmids encoding full-length MyD88. For this assay, we created full-length MyD88 mutants for Sites I-III (R196C, R217A, and K282A/R288A). As shown in Fig. 5A, expression of the full-length MyD88 wild-type in HEK293T cells led to a strong, ligand-independent induction of the NF-κB-dependent luciferase reporter gene. In contrast, expression of the MyD88 mutants, especially R196C and K282A/R288A, led to a significantly reduced induction of the NF-κB-dependent luciferase reporter gene. This result suggests that Sites I, II, and III contribute to interfaces with molecules involved in MyD88 dependent signaling. Among those residues that form Sites I, II, and III, Arg-196 (which forms Site II) has recently been found to be mutated to cysteine in MyD88-deficiency primary immunodeficiency patients (**von Bernuth et al., 2008**). Hence, we analyzed the effect of cysteine substitution of Arg-196 on interaction with the TLR2-TIR using the GST pull-down assay. In this assay, TLR2-TIR was pulled down by the wild-type MyD88-TIR. Interestingly, the Arg-196 substitution by cysteine resulted in a significant decrease in MyD88-TIR affinity for the TLR2-TIR (Fig. 5B). GST pull-down assays were also conducted to analyze the effects of incorporating an alanine substitution of Arg-217 and a double alanine substitution of Lys-282 and Arg-288 (which form Site I and Site III of the MyD88-TIR, respectively) on interactions with the TLR2-TIR. In these assays, the

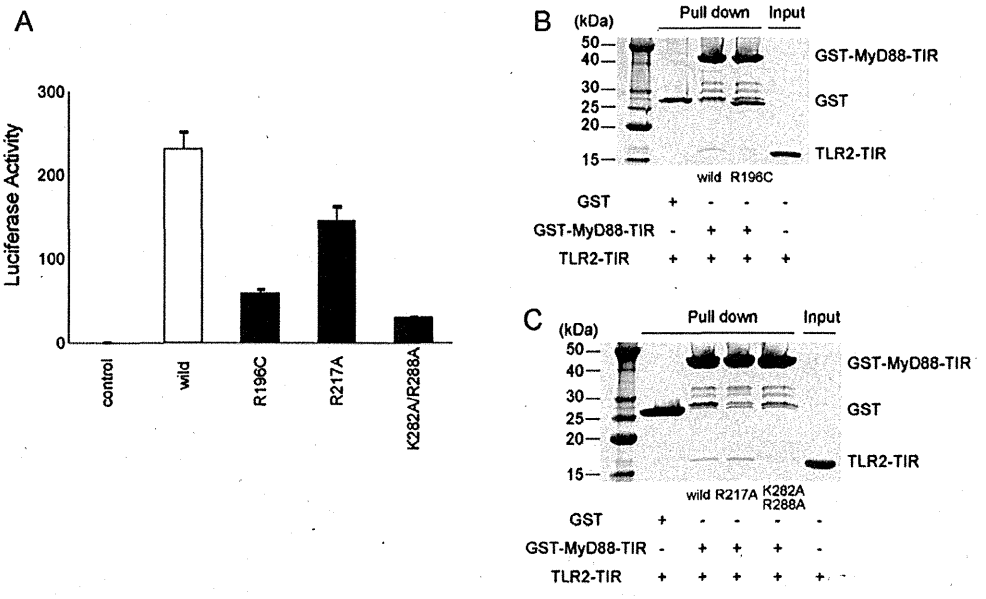

Fig. 5. Functional assay for full-length MyD88 and binding assays for MyD88-TIR mutants with TLR2-TIR. (A) Mutational analysis of MyD88 derived from transfection of HEK293T cells with plasmids encoding the full-length MyD88. Data are shown as the mean + S.D. of quadruplicate wells. Black bars indicate the significantly decreased NF-κB activity, as compared with the wild-type group. The statistical significance of the differences in the luciferase activities between the wild-type and mutants was analyzed using Dunnett's multiple comparison test. Statistical significance was assumed to be $P < 0.05$. (B) Binding assays for wild-type or mutant MyD88-TIRs with TLR2-TIR using GST pull-down assays. The cysteine substitution of Arg-196, which forms Site II, caused a reduced interaction with the TLR2-TIR. (C) The double alanine substitution of Lys-282 and Arg-288, which forms Site III, caused a reduced interaction with TLR2-TIR. The alanine substitution of Arg-217, which forms Site I, had no significant effect.

alanine substitution of Arg-217 had no significant effect. In contrast, the double alanine substitution of Lys-282 and Arg-288 resulted in a significant decrease in MyD88-TIR affinity for the TLR2-TIR (Fig. 5C). These results suggested, therefore, that Site II and Site III, but not Site I, contribute to the interface with TLR2-TIR, as well as with Mal-TIR.

3.4. Similar kinetics of interaction between MyD88, Mal, and TLR2

The binding mode of the TIR domains of MyD88, Mal, TLR1 and TLR2 was analyzed as indicated above (Section 3.1). In addition, we showed that Site II and Site III of the MyD88-TIR served as the binding sites for TLR2-TIR. These two sites also served as binding sites for Mal-TIR in our previous study (Ohnishi et al., 2009). Thus, the present study shows that Site II and Site III of MyD88-TIR form shared binding sites for both TLR2-TIR and Mal-TIR. To analyze mechanisms for the interaction of these TIR proteins, we next evaluated the time-dependent interaction between MyD88, Mal and TLR2 after stimulation with Pam3CSK4 using immunoprecipitation assays. Negative controls consisted of lysates from HEK293T cells, in which expression of TLR2 was not detected, co-transfected with the pcDNA3.1+ myc-tagged MyD88 and pFLAG-CMV6a Mal and stimulated with 0.1 μg/ml Pam3CSK4 for 15 min. In these experiments, stimulation induced the binding activity of MyD88 to TLR2. The binding activity was most significantly enhanced at 30 min post-stimulation. Similarly, the stimulation-induced binding activity of Mal to TLR2 was most significantly enhanced at 15–30 min post-stimulation (Fig. 6). Consequently, these experiments showed that both MyD88 and Mal interacted with TLR2, with the maximal effect occurring 15–30 min after stimulation; this result suggests that these proteins share similar interaction kinetics.

4. Discussion

TIR domains are important signaling modules in TLRs and IL-1/IL-18 signaling events. A TIR domain is typically composed of 135–160 amino acid residues, with the sequence conservation within the domain ranging from 20 to 30%. While the hydrophobic core residues are conserved, the surface exposed residues vary greatly between TIR domains. Consequently, distribution of surface electrostatic potential differs significantly between TIR domains (Dunne et al., 2003), which possibly underlies differences in the binding specificities. Furthermore, recent structural analyses of TIR domain proteins have revealed that the structure of the BB loop, which is considered a functionally important region of TIR domains, differs significantly between TIR domains (Nyman et al., 2008; Ohnishi et al., 2009; Valkov et al., 2011; Xu et al., 2000), suggesting

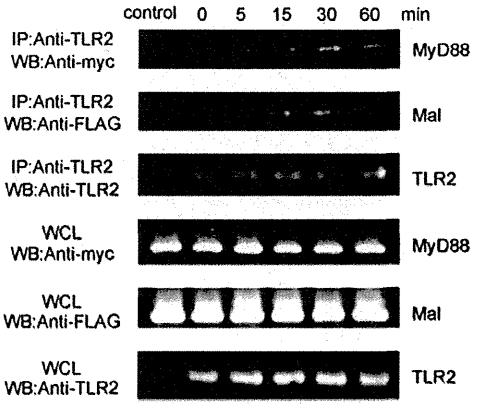

Fig. 6. Time-dependent interaction between MyD88, Mal and TLR2, post-stimulation. The 293-hTLR1/2 cells co-transfected with the pcDNA3.1+ myc-tagged MyD88 and pFLAG-CMV6a Mal were stimulated with 0.1 μg/ml Pam3CSK4 for the indicated intervals. The cell lysates were immunoprecipitated and western blotted. As a negative control, we used lysates from HEK293T cells co-transfected with the pcDNA3.1+ myc-tagged MyD88 and pFLAG-CMV6a Mal and stimulated with 0.1 μg/ml Pam3CSK4 for 15 min. Stimulation with Pam3CSK4 induced the binding activity of MyD88 to TLR2; this activity was most significantly enhanced at 30 min post-stimulation. Similarly, stimulation induced the binding activity of Mal to TLR2, which was most significantly enhanced at 15–30 min post-stimulation.

that the structural deviation of the BB loop might reflect different specificities of the TIR–TIR interaction. Several homotypic interactions have been observed in crystals of TIR domains (Bernoux et al., 2011; Chan et al., 2009; Khan et al., 2004; Tao et al., 2002; Valkov et al., 2011), but heterotypic interactions between TIR–TIR domains have not yet been explained.

We analyzed direct interactions between TIR domains involved in TLR2 signaling using the GST pull-down assay. Mal-TIR directly bound to the TIR domains of receptors (TLR1, TLR2) and MyD88, as well as to TLR4-TIR. In contrast, MyD88-TIR directly bound to the cytosolic TIR domains of TLR1, TLR2, and Mal, but not to TLR4-TIR (Ohnishi et al., 2009) (Fig. 2). These findings are consistent with a previous observation revealed by yeast two-hybrid experiments and GST pull-down assays (Kenny et al., 2009). Thus, these results suggest that hetero-oligomeric TIR–TIR formation between TLR1, TLR2, and adaptors (MyD88 and Mal) is different from that between TLR4 and the same adaptors.

We also identified that three functional surface sites (Sites I–III) of the MyD88-TIR were also important for the Pam3CSK4-activated TLR1/TLR2 signaling pathway, as well as for TLR4 signaling pathway. The alanine substitution of Asp-197, which we previously found to be the functional residue for TLR4 signaling pathway (Ohnishi et al., 2009), resulted in a moderate, but not significant, reduced inhibitory effect in the Pam3CSK4-induced luciferase activity. This indicates that Asp-197 is also likely to be involved in interactions during TLR2 signaling pathway as well as TLR4 signaling pathway (Fig. 3B).

Furthermore, we showed that Sites I, II, and III contributed to interfaces with molecules involved in MyD88 dependent signaling; two of these three functional surface sites, Site II and Site III, served as the binding sites for TLR2-TIR (Fig. 5A–C). Amino acid substitutions may cause unintended global changes in the three-dimensional structures of proteins that can lead to inappropriate conclusions. Therefore, we also examined the purified recombinant proteins using NMR spectroscopy to ensure that no misfolding or global re-arrangements of TIR domains had occurred (Fig. 4A). The residues for which the cross-peaks disappeared in the original position of the wild-type MyD88-TIR in the 2D ^{1}H–^{15}N correlation spectra of the mutant proteins reside close to Arg-196, Arg-217, Lys-282, or Arg-288 (Fig. 4B). This indicates that introduction of the mutations did not affect the overall folding of the domain structures. Interestingly, the two sites have also served as the binding sites for Mal-TIR in our previous study (Ohnishi et al., 2009). Thus, the present study shows that Site II and Site III of MyD88-TIR serve as shared binding sites for both TLR2-TIR and Mal-TIR. Arg-217 in Site I played a crucial role in the TLR2-mediated cellular response to Pam3CSK4 stimulation, but was not involved in direct binding to TLR2. This site has also not been involved in direct binding to Mal-TIR, and the direct interaction of MyD88-TIR with the death domain of IRAK4 was not observed in our previous study (Ohnishi et al., 2009). We demonstrated that the alanine substitution of Arg-217 resulted in no significant decrease in MyD88-TIR affinity for the TLR1-TIR (data not shown). Therefore, Site I may have no involvement in, or make minimal contributions to, interfaces with the TIR domains in TLR1/TLR2 signaling.

We next investigated the time-dependent interaction between MyD88, Mal and TLR2 post-stimulation. This experiment showed that the interaction kinetics of TLR2 with MyD88 was similar to that observed for Mal (Fig. 6). Therefore, it is possible that MyD88 and Mal bind to identical or different TLR2 molecules and share similar interaction kinetics. The crystal structure of the MyD88-IRAK4-IRAK2 death domain complex has recently been reported (Lin et al., 2010). The structure reveals a helical oligomer (called a Myddosome), which consists of six MyD88, four IRAK-4 and four IRAK-2 death domains. As this structure, an unknown complicated assembly of the TIR domains, including MyD88, Mal, TLR1, and TLR2, may form the higher order oligomer.

Primary immuno-deficiency syndromes with innate immune defects have recently been defined (Notarangelo et al., 2009). The phenotypes characteristic of IRAK-4 deficiency and MyD88 deficiency suggest that the Gram-positive bacterial recognition system is dependent on the TLR2/Mal/MyD88/IRAK-4 signaling cascade, indicating that it is important to consider the links between protein functions and gene mutations in the TLR2 signaling pathway. Most gene variations in IRAK-4 deficiency and MyD88 deficiency cause the loss of stability of proteins or the deletion of proteins (Conway et al., 2010; Ku et al., 2007; von Bernuth et al., 2008). We focused on the Site II residue, Arg196 of MyD88, which has been found to be mutated to cysteine in MyD88 deficiency patients (von Bernuth et al., 2008). The 2D ^{1}H–^{15}N correlation spectrum showed that the residues for which the cross-peaks were shifted by the cysteine substitution at Arg-196 reside close to Arg-196. In these residues, F164, I165, C168 are all located distant in the sequence, but proximal in space to Arg-196 (Fig. 4B). This indicates that introduction of the mutation did not affect the overall folding of the domain structure, although it would be expected to exert a minor effect on the BB loop that connects the second β-strand and second helix and consists of residues 194–208, owing to its proximity. Consequently, the Arg-196 substitution did not cause destabilization of the MyD88-TIR protein. However, this missense mutation caused a significant decrease in the direct binding ability to TLR2-TIR as well as to Mal-TIR (Fig. 4A) (Ohnishi et al., 2009). The loss of interactions of MyD88-TIR with TLR2-TIR or Mal-TIR caused by the mutation would be a critical molecular factor influencing the specific phenotype of MyD88 deficiency patients. Thus, this result may provide a molecular explanation of the symptoms experienced by MyD88 deficiency patients.

In conclusion, we have demonstrated that MyD88-TIR directly binds to TLR2-TIR, but not to TLR4-TIR. We have also shown that two isolated sites in the MyD88-TIR mediate direct interactions with TLR2-TIR and that these sites are shared with Mal-TIR. The interaction kinetics for TLR2 with MyD88 is similar to TLR2 with Mal. Identification of the MyD88 residues that are involved in direct interactions with TLR2 is of clinical significance because of the association of one of these residues with primary immunodeficiency syndrome. The mechanism of TLR2 signaling initiation remains to be clarified by further studies. However, we believe that the novel information on the binding mode of the TIR proteins provided by this study will facilitate future structural determination of hetero-oligomeric TIR domain complexes.

Acknowledgments

We thank Dr. Tokumi, T., Souma, W., Tsuji, K., and Kasahara, K. for their technical help. This work was supported by Grants-in-Aid for Scientific Research from the Ministry of Education, Culture, Sports, Science and Technology of Japan and by Health and Labour Science Research Grants for Research on Intractable Diseases from the Ministry of Health, Labour and Welfare.

Appendix A. Supplementary data

Supplementary data associated with this article can be found, in the online version, at http://dx.doi.org/10.1016/j.molimm.2012.05.003.

References

Akira, S., Uematsu, S., Takeuchi, O., 2006. Pathogen recognition and innate immunity. Cell 124, 783–801.

Arbour, N.C., Lorenz, E., Schutte, B.C., Zabner, J., Kline, J.N., Jones, M., Frees, K., Watt, J.L., Schwartz, D.A., 2000. TLR4 mutations are associated with endotoxin hyporesponsiveness in humans. Nature Genetics 25, 187–191.

Bernoux, M., Ve, T., Williams, S., Warren, C., Hatters, D., Valkov, E., Zhang, X., Ellis, J.G., Kobe, B., Dodds, P.N., 2011. Structural and functional analysis of a plant resistance protein TIR domain reveals interfaces for self-association, signaling, and autoregulation. Cell Host Microbe 9, 200–211.

Chan, S.L., Low, L.Y., Hsu, S., Li, S., Liu, T., Santelli, E., Negrate, G.L., Reed, J.C., Woods Jr., V.L., Pascual, J., 2009. Molecular mimicry in innate immunity: crystal structure of a bacterial TIR domain. Journal of Biological Chemistry 284, 21386–21392.

Conway, D.H., Dara, J., Bagashev, A., Sullivan, K.E., 2010. Myeloid differentiation primary response gene 88 (MyD88) deficiency in a large kindred. Journal of Allergy and Clinical Immunology 126, 172–175.

Delaglio, F., Grzesiek, S., Vuister, G., Zhu, G., Pfeifer, J., Bax, A., 1995. NMRPipe: a multidimensional spectral processing system based on UNIX pipes. Journal of Biomolecular NMR 6, 277–293.

Dunne, A., Ejdeback, M., Ludidi, P.L., O'Neill, L.A.J., Gay, N.J., 2003. Structural complementarity of Toll/interleukin-1 receptor domain in Toll-like receptors and the adaptors Mal and MyD88. Journal of Biological Chemistry 278, 41443–41451.

Goddard, T.D., Kneller, D.G., 1999. SPARKY 3. University of California, San Francisco.

Guan, Y., Ranoa, D.R.E., Jiang, S., Mutha, S.K., Li, X., Baudry, J., Tapping, R.I., 2010. Human TLRs10 and 1 share common mechanisms of innate immune sensing but not signaling. Journal of Immunology 184, 5094–5103.

Horng, T., Barton, G.M., Flavell, R.A., Medzhitov, R., 2002. The adaptor molecule TIRAP provides signaling specificity for Toll-like receptors. Nature 420, 329–333.

Kagan, J.C., Medzhitov, R., 2006. Phosphoinositide-mediated adaptor recruitment controls Toll-like receptor signaling. Cell 125, 943–955.

Kaisho, T., Akira, S., 2006. Toll-like receptor function and signaling. Journal of Allergy and Clinical Immunology 117, 979–987.

Kawai, T., Akira, S., 2007. Signaling to NF-κB by Toll-like receptors. Trends in Molecular Medicine 13, 460–469.

Kenny, E.F., Talbot, S., Gong, M., Golenbock, D.T., Bryant, C.E., O'Neill, L.A.J., 2009. MyD88 adaptor-like is not essential for TLR2 signaling and inhibits signaling by TLR3. Journal of Immunology 183, 3642–3651.

Khan, J.A., Brint, E.K., O'Neill, L.A.J., Tong, L., 2004. Crystal structure of the Toll/interleukin-1 receptor domain of human IL-1RAPL. Journal of Biological Chemistry 279, 31664–31670.

Khor, C.C., Chapman, S.J., Vannberg, F.O., Dunne, A., Murphy, C., Ling, E.Y., Frodsham, A.J., Walley, A.J., Kyrieleis, O., Khan, A., Aucan, C., Segal, S., Moore, C.E., Knox, K., Campbell, S.J., Lienhardt, C., Scott, A., Aaby, P., Sow, O.Y., Grignani, R.T., Sillah, J., Sirugo, G., Peshu, N., Williams, T.N., Maitland, K., Davies, R.J.O., Kwiatkowski, D.P., Day, N.P., Yala, D., Crook, D.W., Marsh, K., Berkley, J.A., O'Neill, L.A.J., Hill, A.V.S., 2007. A Mal functional variant is associated with protection against invasive pneumococcal disease, bacteremia, malaria and tuberculosis. Nature Genetics 39, 523–528.

Ku, C.L., von Bernuth, H., Picard, C., Zhang, S.Y., Chang, H.H., Yang, K., Chrabieh, M., Issekutz, A.C., Cunningham, C.K., Gallin, J., Holland, S.M., Roifman, C., Ehl, S., Smart, J., Tang, M., Barrat, F.J., Levy, O., McDonald, D., Day-Good, N.K., Miller, R., Takada, H., Hara, T., Al-Hajjar, S., Al-Ghonaium, A., Speert, D., Sanlavillle, D., Li, X., Geissmann, F., Vivier, E., Maródi, L., Garty, B.Z., Chapel, H., Rodriguez-Gallego, C., Bossuyt, X., Abel, L., Puel, A., Casanova, J.L., 2007. Selective predisposition to bacterial infections in IRAK-4-dedicient children: IRAK-4-dependent TLRs are otherwise redundant in protective immunity. Journal of Experimental Medicine 204, 2407–2422.

Lin, S.C., Lo, Y.C., Wu, H., 2010. Helical assembly in the MyD88-IRAK4-IRAK2 complex in TLR/IL-1R signaling. Nature 465, 885–890.

Notarangelo, L.D., Fischer, A., Geha, R.S., Casanova, J.L., Chapel, H., Conley, M.E., Cunningham-Rundles, C., Etzioni, A., Hammarström, L., Nonoyama, S., Ochs, H.D., Puck, J., Roifman, C., Seger, R., Wedgwood, J., 2009. Primary immunodefiencies: 2009 update. Journal of Allergy and Clinical Immunology 124, 1161–1178.

Nyman, T., Stenmark, P., Flodin, S., Johansson, I., Hammarstrm, M., Nordlund, P., 2008. The crystal structure of the human Toll-like receptor 10 cytoplasmic domain reveals a putative signaling dimer. Journal of Biological Chemistry 283, 11861–11865.

Ohnishi, H., Tochio, H., Kato, Z., Orii, K.E., Li, A., Kimura, T., Hiroaki, H., Kondo, N., Shirakawa, M., 2009. Structual basis for the multiple interaction of the MyD88 TIR domain in TLR4 signaling. Proceedings of the National Academy of Sciences of the United States of America 106, 10260–10265.

Ohnishi, H., Tochio, H., Kato, Z., Kimura, T., Hiroaki, H., Kondo, N., Shirakawa, M., 2010. 1H, 13C, and 15N resonance assignment of the TIR domain of human MyD88. Biomolecular NMR Assignments 2, 123–125.

O'Neill, L.A., Bowie, A.G., 2007. The family of five: TIR-domain-containing adaptors in Toll-like receptor signaling. Nature Reviews Immunology 7, 353–364.

Picard, C., Casanova, J.L., Puel, A., 2011. Infectious disease in patients with IRAK-4, MyD88, NEMO, or IκBα deficiency. Clinical Microbiology Reviews 24, 490–497.

Santos-Sierra, S., Deshmukh, S.D., Kalnitski, J., Küenzi, P., Wymann, M.P., Golenbock, D.T., Hanneke, P., 2009. Mal connects TLR2 to PI3Kinase activation and phagocyte polarization. EMBO Journal 28, 2018–2027.

Schanda, P., Brutscher, B., 2005. Very fast two-dimensional NMR spectroscopy for real-time investigation of dynamic events in proteins on the time scale of seconds. Journal of the American Chemical Society 127, 8014–8015.

Tao, X., Xu, Y., Zheng, Y., Beg, A.A., Tong, L., 2002. An extensively associated dimer in the structure of the C713S mutant of the TIR domain of human TLR2. Biochemical and Biophysical Research Communications 299, 216–221.

Tao, X., Tong, L., 2009. Expression, purification, and crystallization of Toll/interleukin-1 receptor (TIR) domains. Methods in Molecular Biology 517, 81–88.

Ulrichts, P., Peelman, F., Beyaert, R., Tavernier, J., 2007. MAPPIT analysis of TLR adaptor complexes. FEBS Letters 581, 629–636.

Valkov, E., Stamp, A., DiMaio, F., Baker, D., Verstak, B., Roversi, P., Kellie, S., Sweet, M.J., Mansell, A., Gay, N.J., Martin, J.L., Kobe, B., 2011. Crystal structure of Toll-like receptor adaptor MAL/TIRAP reveals the molecular basis for signal transduction and disease protection. Proceedings of the National Academy of Sciences of the United States of America 108, 14879–14884.

von Bernuth, H., Picard, C., Jin, Z., Pankla, R., Xiao, H., Ku, C.L., Chrabieh, M., Mustapha, I.B., Ghandil, P., Camcioglu, Y., Vasconcelos, J., Sirvent, N., Guedes, M., Vitor, A.B., Herrero-Mata, M.J., Aróstegui, J.I., Rodrigo, C., Alsina, L., Ruiz-Ortiz, E., Juan, M., Fortuny, C., Yagüe, J., Antón, J., Pascal, M., Chang, H.H., Janniere, L., Rose, Y., Garty, B.Z., Chapel, H., Issekutz, A., Maródi, L., Rodriguez-Gallego, C., Banchereau, J., Abel, L., Li, X., Chaussabel, D., Puel, A., Casanova, J.L., 2008. Pyogenic bacterial infections in humans with MyD88 deficiency. Science 321, 691–696.

Xu, Y., Tao, X., Shen, B., Horng, T., Medzhitov, R., Manley, J.L., Tong, L., 2000. Structural basis for signal transduction by the Toll/interleukin-1 receptor domains. Nature 408, 111–115.

J Clin Immunol
DOI 10.1007/s10875-012-9744-6

ORIGINAL RESEARCH

Autosomal-Dominant Chronic Mucocutaneous Candidiasis with *STAT1*-Mutation can be Complicated with Chronic Active Hepatitis and Hypothyroidism

Tomohiro Hori · Hidenori Ohnishi · Takahide Teramoto · Kohji Tsubouchi · Takafumi Naiki · Yoshinobu Hirose · Osamu Ohara · Mariko Seishima · Hideo Kaneko · Toshiyuki Fukao · Naomi Kondo

Received: 21 May 2012 / Accepted: 16 July 2012

Abstract
Purpose To describe a case of autosomal-dominant (AD)-chronic mucocutaneous candidiasis (CMC) with a signal transducer and activator of transcription (STAT) 1 gene mutation, and some of the important complications of this disease such as chronic hepatitis.
Methods We present a 23-year-old woman with CMC, chronic active hepatitis, and hypothyroidism. Her father also had CMC. We performed several immunological analyses of blood and liver samples, and searched for gene mutations for CMC in the patient and her father.
Results We identified the heterozygous substitution c.821 G >A (p.Arg274Gln) in the *STAT1* gene of both the patient and her father. The level of β-glucan induced interferon (IFN)-γ in her blood cells was significantly low. Immunoblot analysis detected serum anti-interleukin (IL)-17 F autoantibody. She was found to have increased (low-titer) antibodies related to her hypothyroidism and hepatitis. Her serum IL-18 levels fluctuated with her AST and ALT levels. Liver biopsy revealed CD68-positive cell infiltration and IL-18 expression in the sinusoidal regions. These results suggest that the chronic active hepatitis in this patient may be exacerbated by the excessive IL-18 accumulation caused by recurrent mucocutaneous fungal infection, and decreased IFN-γ production.
Conclusions AD-CMC is known to be caused by a gain-of-function mutation of the *STAT1* gene. Chronic active hepatitis is a rare complication of AD-CMC, with currently unknown pathogenesis. It seems that the clinical phenotype in this patient is modified by autoimmune mechanisms and cytokine dysregulation. AD-CMC can be complicated by various immune disorders including autoimmune polyendocrinopathy-candidiasis-ectodermal dystrophy.

Keywords AD-CMC · STAT1 · hypothyroidism · chronic active hepatitis · anti-IL-17 F autoantibody · IL-18

T. Hori · H. Ohnishi (✉) · T. Teramoto · T. Fukao · N. Kondo
Department of Pediatrics, Graduate School of Medicine,
Gifu University,
1-1 Yanagido,
Gifu 501-1194, Japan
e-mail: ohnishih@gifu-u.ac.jp

K. Tsubouchi
Department of Pediatrics, Chuno Kosei Hospital,
Gifu, Japan

T. Naiki
Department of Gastroenterology, Graduate School of Medicine,
Gifu University,
Gifu, Japan

Y. Hirose
Department of Pathology, Gifu University Hospital,
Gifu, Japan

O. Ohara
Laboratory for Immunogenomics,
RIKEN Research Center for Allergy and Immunology,
Yokohama, Japan

O. Ohara
Department of Human Genome Research,
Kazusa DNA Research Institute,
Kisarazu, Japan

M. Seishima
Department of Dermatology, Graduate School of Medicine,
Gifu University,
Gifu, Japan

H. Kaneko
Department of Clinical Research, Nagara Medical Center,
Gifu, Japan

Published online: 31 July 2012

Abbreviations

AD	Autosomal dominant
AIRE	Autoimmune regulator
ANA	Antinuclear antibody
APECED	Autoimmune polyendocrinopathy-candidiasis-ectodermal dystrophy
AR	Autosomal recessive
ASMA	Anti-smooth muscle antibody
CARD	Caspase recruitment domain-containing protein
CMC	Chronic mucocutaneous candidiasis
DOCK	Dedicator of cytokinesis
GAF	Interferon-γ activating factor
HIES	Hyper-IgE syndrome
IFN	Interferon
IL	Interleukin
ISGF3	Interferon-stimulated-γ factor 3
LKM-1	Liver-kidney microsome 1
MSMD	Mendelian susceptibility to mycobacterial disease
PBMCs	Peripheral blood mononuclear cells
PHA	Phytohemagglutinin
STAT	Signal transducer and activator of transcription
TNF	Tumor necrosis factor
TPOAb	Anti-thyroid peroxidase antibody
TSBAb	Thyroid stimulating hormone blocking antibody

Introduction

Chronic mucocutaneous candidiasis (CMC) is characterized by susceptibility to candida infections of the skin, nails, and mucous membranes. CMC is caused by inborn errors of interleukin (IL)-17 immunity [1], due to mutations of the autoimmune regulator (*AIRE*) gene that cause autoimmune polyendocrinopathy-candidiasis-ectodermal dystrophy (APECED) [2–4], the signal transducer and activator of transcription-3 (*STAT3*) gene that cause autosomal dominant (AD)-hyper-IgE syndrome (HIES) [5], the dedicator of cytokinesis-8 (*DOCK8*) gene that cause autosomal recessive (AR)-HIES [6], the caspase recruitment domain-containing protein-9 (*CARD9*) gene [7], the IL-17 receptor-A (*IL17RA*) gene, the *IL17F* gene [1], or the *STAT1* gene [8, 9].

STAT1 has an essential role in the interferon (IFN)-γ and type I interferon-receptor signaling pathways. In response to IFN-γ stimulation, STAT1 forms homodimers or heterodimers with STAT3 that bind to the IFN-γ activation site promoter element (IFN-γ activating factor, GAF). In response to IFN-α or IFN-β stimulation, STAT1 forms a heterodimer with STAT2 that can bind to the interferon-stimulated response element (IFN-stimulated-γ factor 3, ISGF3) [10].

Loss of function of the *STAT1* gene results in Mendelian susceptibility to mycobacterial disease (MSMD) [11]. In 2011, the gain-of-function mutation of *STAT1* was shown to cause AD-CMC [8, 9]. Here, we report a family with AD-CMC and *STAT1* mutation, and show that chronic active hepatitis and hypothyroidism may be associated with this specific condition.

Methods

Patients

The patient is now a 23-year-old female. She first consulted us at age 11 years because of chronic candidiasis of her skin, nails, and oral cavity that she had experienced since the age of 3 years. She had short stature (3 standard deviations below the mean), myxedematous fingers, and puffy lips. Her thyroid was described as atrophic on ultrasonography. Her father also had a history of CMC since childhood. He had a history of smoking and alcohol ingestion, and had died of oral cancer (squamous cell carcinoma) at the age of 49 years. The results of laboratory examinations are shown in Table I. She had hypothyroidism and liver dysfunction. Anti-thyroid peroxidase antibody (TPOAb) was positive. Testing for hepatitis-associated autoantibodies revealed positive serum antinuclear antibody (ANA) at the first visit and at age 22 years, and positive (low-titer) serum anti-smooth muscle antibody (ASMA) and anti-liver-kidney microsome 1 (LKM-1) antibody at age 22 years, but anti-mitochondrial antibody was negative. Serum markers for hepatitis virus were negative.

Oral administration of levothyroxine (100 μg/day) improved her growth rate. Her liver function deteriorated (AST 560 IU/L, ALT 1040 IU/L) at age 12 years and liver biopsy revealed chronic active hepatitis with piecemeal necrosis. She was diagnosed with autoimmune hepatitis according to the International Autoimmune Hepatitis Group criteria (1999) [12]. Her liver function improved with administration of oral prednisolone for 17 months followed by oral azathioprine (100 mg/day).

Analysis of Gene Mutations

Genomic DNA was extracted from leukocytes (except from the patient's deceased father, whose DNA was extracted from stored skin tissue) using SepaGene (EIDIA, Tokyo, Japan). DNA fragments of the *AIRE* and *STAT1* genes were amplified by polymerase chain reaction, and analyzed using big dye terminator bidirectional sequencing (Applied Biosystems, Foster City, CA, USA).

Cell Culture

Peripheral blood mononuclear cells (PBMCs) were isolated from the heparinized blood of control donors and the patient

Table I Laboratory examination results

		Reference value	11 years old (first presentation)	22 years old (re-presentation)
TSH	(μIU/mL)	0.35–4.94	622	201.3
FT3	(pg/mL)	1.71–3.71	0.55	1.45
FT4	(μg/dL)	0.70–1.48	0.06	0.24
TPOAb (RIA)	(IU/mL)	<0.3	8.6	NP
TPOAb (ECLIA)	(IU/mL)	<16	NP	23
TgAb			ND	ND
TRAb			ND	ND
TSBAb			ND	ND
AST	(IU/L)	7–35	137	124
ALT	(IU/L)	7–40	159	169
LDH	(IU/L)	125–225	885	206
ANA		<1:40	1:160	1:80
AMA			ND	ND
ASMA		<1:40	ND	1:40
anti-LKM-1 antibody	(index)	a	NP	26
IgG	(mg/dL)	890–1850	1947	1928
IgA	(mg/dL)	95–460	176	289
IgM	(mg/dL)	45–300	414	532
Lymphocytes subsets				
CD3	(%)	65.0–85.0	NP	78.4
CD4	(%)	35.0–65.0	NP	44.2
CD8	(%)	20.0–35.0	NP	35.7
CD19	(%)	5.0–15.0	NP	7.4
Lymphocyte proliferation assay				
no stimulus	(cpm)	127–459	NP	179
PHA	(cpm)	20500–56800	NP	42800
Con A	(cpm)	20300–65700	NP	38000
neutrophil phagocytosis function	(%)	70–87	NP	91.6
neutrophil sterilizing function	(%)	93–97	NP	89.6
natural killer cells activity	(%)	18–40	NP	50

TSH thyroid-stimulating hormone, *FT3* free triiodothyronine, *FT4* free thyroxine, *TPOAb* anti-thyroid peroxidase antibody, *TgAb* anti-thyroglobulin antibody, *TRAb* thyroid stimulating hormone receptor antibody, *TSBAb* thyroid stimulating hormone blocking antibody, *AST* aspartate aminotransferase, *ALT* alanine aminotransferase, *LDH* lactate dehydrogenase, *ANA* antinuclear antibody, *AMA* anti-mitochondrial antibody, *ASMA* anti-smooth muscle antibody, *LKM-1* liver-kidney microsome 1, *PHA* phytohemagglutinin, *Con A* concanavalin A, *IL* interleukin, *IFN* interferon, *PBMCs* peripheral blood mononuclear cells, *ECLIA* electrochemiluminescence immunoassay, *RIA* radioimmunoassay

ND not detected, *NP* not performed

[a] <17: negative, 17–49: indeterminate, >49: positive

by gradient centrifugation using Ficoll-Paque (GE Healthcare, Uppsala, Sweden). The PBMCs were cultured in medium consisting of RPMI 1640 supplemented with 10 % heat-inactivated fetal calf serum, L-glutamine (2 mmol/L), penicillin (100 U/mL), and streptomycin (100 μg/mL).

PBMCs were seeded to a density of 10^6 per mL, and cultured in the presence or absence of 10 μg/mL of phytohemagglutinin (PHA) (GIBCO, Life Technologies Corp., Grand Island, NY, USA) and 300 μg/mL of curdlan (β-1,3-glucan; Wako Pure Chemical Industries, Osaka, Japan) for 72 h in 24-well plates at 37 °C in a humidified atmosphere at 5 % CO_2.

Analysis of Cytokine Levels by ELISA

Serum samples were stored at −80 °C until assayed. Culture supernatants in test tubes or microtest plates were centrifuged to remove cells and stored at −80 °C until assayed. IFN-γ concentrations were measured with a human IFN-γ analysis kit (Otsuka Pharmaceutical Co., Tokyo, Japan) with a detection limit of 2 pg/mL. Similarly, tumor necrosis factor (TNF)-α concentrations were measured with an immunoassay kit (BioSource International, Carlsbad, CA, USA) with a detection limit of 1.7 pg/mL. IL-18 was assayed by ELISA (MBL, Nagoya, Japan), with a detection limit of 25.6 pg/mL.

Immunoblot Analysis

Recombinant IL-17 A, IL-17 F, and IL-22 (R&D Systems, Minneapolis, MN, USA) were electrophoresed on 15 % gel (XV Pantera gel, DRC Corp., Tokyo, Japan). Separated proteins were then transferred onto membranes using an iBot system (Invitrogen Corp., Carlsbad, CA, USA) at 30 mA for 14 min. The membranes were blocked with

blocking buffer (20 mM Tris, pH 7.5, 150 mM NaCl, 3 % BSA) for 1 h at room temperature. After two 5-min washes in TBS-T (10 mM Tris, pH 8.0, 150 mM NaCl, 0.1 % Tween20), they were reacted with the patient's sera for 1 h. After washing four times, the membranes were incubated with goat anti-human IgG conjugated to HRP (1:3,000). Detection was performed using ECL-plus (Amersham, Piscataway, NJ, USA) and a light capture system (AE6970CP; ATTO, Tokyo, Japan). Additional immunoblot analyses were performed using the patient's serum neutralized by the antigenic proteins, and the sera of healthy control subjects, to confirm the staining band as IL-17 F. The neutralizing serum was produced by mixing 40 μL of the patient's serum with 1,250 ng of the antigenic proteins, and incubating for 24 h. Each 250 ng of the antigenic proteins was electrophoresed on 15 % gel.

Immunohistochemistry

The patient's liver biopsy specimen was histologically examined after hematoxylin-eosin and immunohistochemical staining. Hepatic immunohistochemical staining was performed as previously described [13]. Immunohistochemical analysis of IL-18 expression was performed with an antihuman IL-18 monoclonal antibody, clone CPTC-IL18-1 (Millipore, Billerica, MA, USA). Mouse monoclonal anti-CD68 antibody clone KP1 (Dako, Glostrup, Denmark) was used as another primary antibody. Replacement of the primary antibody with Mouse IgG1 K Isotype Control Purified (eBioscience, San Diego, CA, USA) resulted in negative staining.

Results

Identification of the Patient's Pathogenic Gene Mutation

We initially considered APECED (also known as autoimmune polyendocrinopathy type 1) as a possible diagnosis. This multi-organ autoimmune disease with CMC is caused by mutation of the *AIRE* gene [2, 3]. Hypoparathyroidism, adrenal failure, and CMC are three major hallmarks of this disease [14]. In 2011, van de Veerdonk et al. and Liu et al. reported that the gain-of-function mutation of *STAT1* caused AD-CMC [8, 9]. We therefore analyzed the *AIRE* and *STAT1* genes in the patient and her father.

We identified the homozygous polymorphism c.961 C>G (p.Ser278Arg) in the patient's *AIRE* gene. However, no pathogenic mutation was found in *AIRE*. We eventually identified the heterozygous substitution c.821 G>A (p.Arg274Gln) in the *STAT1* gene of both the patient and her father. Liu et al. reported that this mutation caused AD-CMC [9]. We therefore concluded that CMC was caused by the *STAT1* mutation in this family.

Immunological Analyses

Analysis of the patient's IFN-γ, TNF-α, and IL-18 production levels by PBMCs after β-glucan or PHA stimulation revealed that her β-glucan-stimulated IFN-γ production was significantly lower than that of age-matched healthy controls, although PHA-stimulated IFN-γ production and β-glucan-stimulated TNF-α and IL-18 production were not significantly different compared with healthy controls (Fig. 1).

We analyzed anti-IL-17 antibody in the patient's serum because it has been reported that the anti-IL-17 family of autoantibodies may contribute to the pathogenesis of CMC in APECED [4]. Immunoblot analysis showed anti-IL-17 F autoantibody in her serum, but not anti-IL-17 A or anti-IL-22 autoantibodies (Fig. 2a). Moreover, her serum neutralized by IL-17 F had lower reactivity than her non-neutralized serum, and the control was negative (Fig. 2b). We therefore considered that this staining band indicated the presence of anti-IL-17 F autoantibody.

When she re-visited our hospital at age 22 years we were able to evaluate her immunological status, as she had not taken medication for more than 6 months. At that time, she had increased serum immunoglobulin levels (Table I). Analysis of her serum IL-18 levels, liver enzyme levels, and liver tissue at the time of exacerbation of hepatitis revealed that her IL-18 levels fluctuated with AST and ALT levels (serum IL-18 level in age-matched healthy controls is 189±82 pg/mL) (Fig. 3). Histological examination of her liver biopsy specimen after hematoxylin-eosin staining strongly suggested the presence of chronic active hepatitis because of the features of interface hepatitis with a heavy infiltrate of plasma cells in the portal tracts, and the absence of abnormal angiogenesis. Additionally, CD68-positive cell infiltration and IL-18 expression were seen in the sinusoidal regions (Fig. 4).

Discussion

We present a case of AD-CMC with *STAT1* mutation complicated by chronic active hepatitis and hypothyroidism. Previous studies indicated that AD-CMC patients with *STAT1* mutation have a relatively high frequency of hypothyroidism and other rare disorders. Our patient's chronic active hepatitis is a rare complication compared with 61 other AD-CMC patients with *STAT1* mutation [8, 9].

The pathogenesis of CMC is generally thought to have two possible mechanisms: impaired IL-17-mediated immunity and secondary immunodeficiency due to anti-IL-17 autoantibodies. Liu et al. and Smeekens et al. reported that the gain-of-function mutation of *STAT1* causes AD-CMC by impairing IL-17-mediated immunity [9, 15]. The constitutively activated

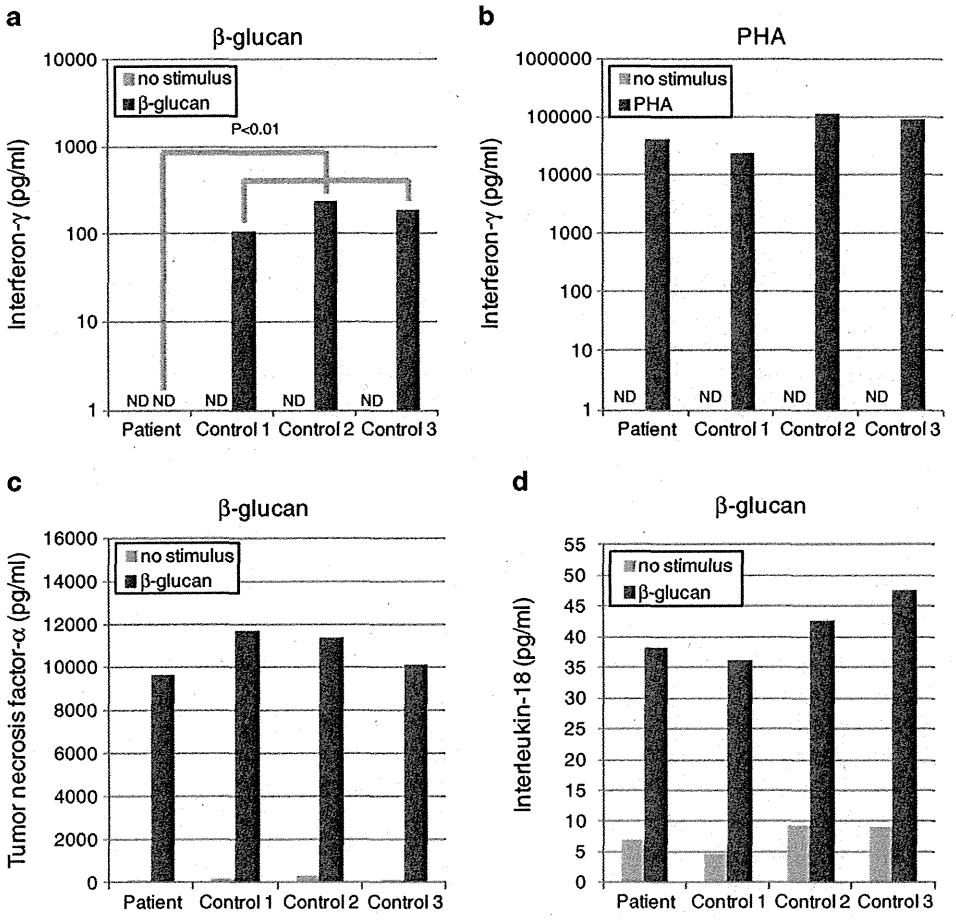

Fig. 1 IFN-γ, TNF-α, and IL-18 production by peripheral blood mononuclear cells after β-glucan or phytohemagglutinin stimulation. The patient's β-glucan-stimulated IFN-γ production was significantly lower than that of age-matched healthy controls **(a)**. Phytohemagglutinin-stimulated IFN-γ production and β-glucan-stimulated TNF-α and IL-18 production did not show significant differences compared with healthy controls **(b, c, d)**. *ND*, Not detected

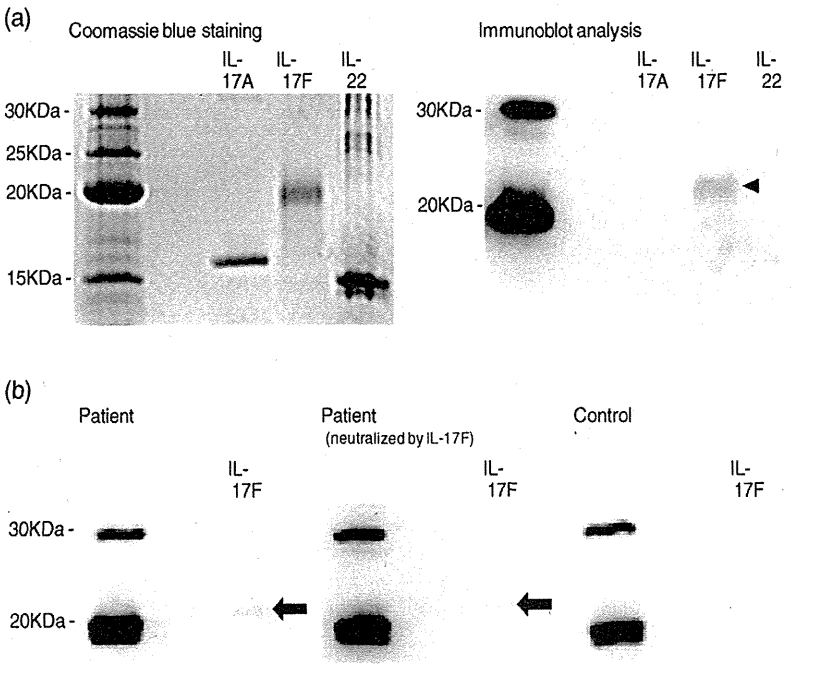

Fig. 2 Immunoblot analysis of autoantibodies against IL-17 A, IL-17 F, and IL-22. The patient's serum was positive for anti-IL-17 F autoantibody (*arrowhead*), but not anti-IL-17 A or anti-IL-22 autoantibodies **(a)**. For immunoblot analysis of autoantibodies against IL-17 F, the patient's serum was compared with her serum neutralized by IL-17 F antigen and the serum of control subjects. Her serum neutralized by IL-17 F had a lower reactivity than the non-neutralized serum (*arrows*). The control was negative **(b)**

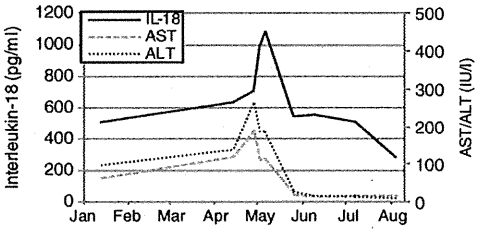

Fig. 3 Time-course of serum AST, ALT, and IL-18 levels. The patient's serum IL-18 levels were elevated due to her hepatitis (levels in age-matched healthy controls are 189±82 pg/mL)

STAT1 mutants are dephosphorylated. Cellular responses may then cause an imbalance between STAT1-dependent signaling and STAT3-dependent signaling, and suppress the development of T cells producing IL-17 A, IL-17 F, and IL-22. The candidiasis is probably explained by subsequent impaired β-defensin production (which should be driven by IL-22) and a lack of local neutrophil response and activation. Van de Veerdonk et al. reported that the mononuclear cells of AD-CMC patients with *STAT1* mutation were characterized by poor production of IFN-γ, IL-17, and IL-22, suggesting defects within the IL-12 and IL-23 receptor signaling pathways [8]. The cytokine production patterns in our patient were similar to those in the AD-CMC patients with *STAT1* mutation reported by van de Veerdonk et al. [8] (Fig. 1). This specific cellular response seems to be associated with the pathogenesis of CMC caused by mutated *STAT1*. However, it has also been reported that the suppression of IL-17 function causes secondary immunodeficiency and CMC in APECED [4]. The importance of IL-17 in the pathogenesis of CMC is also supported by the fact that *IL17RA* and *IL17F* gene mutations have been shown to cause CMC [1]. Interestingly, our patient had anti-IL-17 F autoantibodies (Fig. 2), as in APECED. Both poor β-glucan stimulated IFN-γ production and anti-IL-17 F antibodies may be contributing to the clinical manifestations in our patient. These findings in STAT-1 deficiency cast some doubt on this putative mechanism for CMC in APECED. The pathogenic mechanisms of immunodeficiency which cause candidiasis in APECED may result from both suppression of IL-17 function and some kind of cytokine dysregulation.

Hypothyroidism caused by a mutated *STAT1* gene may be associated with thyroid autoantibodies. Van de Veerdonk et al. reported that of 14 patients with AD-CMC with *STAT1* mutations, 3 had hypothyroidism, 2 of whom were positive for thyroid autoantibodies, and 1 additional patient with normal thyroid function also tested positive for thyroid autoantibodies [8]. The reason that the *STAT1* mutation causes hypothyroidism is as follows. It is known that thyrotropin induces production of suppressor of cytokine signaling 1, which in turn alters STAT1 phosphorylation. Thyrotropin may act as a cytokine inhibitor in thyroid tissue, and mutated *STAT1* may inhibit the rescue of thyroid cells by thyrotropin and contribute to hypothyroidism [8, 16]. In our patient, the thyroid gland was atrophic, and TPOAb, but not thyroid stimulating hormone blocking antibody (TSBAb), was detected in her serum. TPOAb is known to be a major pathogenic factor in chronic (Hashimoto's) thyroiditis. Some patients with this disorder have been reported to have atrophic thyroiditis [17]. TSBAb is also known to cause hypothyroidism in patients with atrophic autoimmune

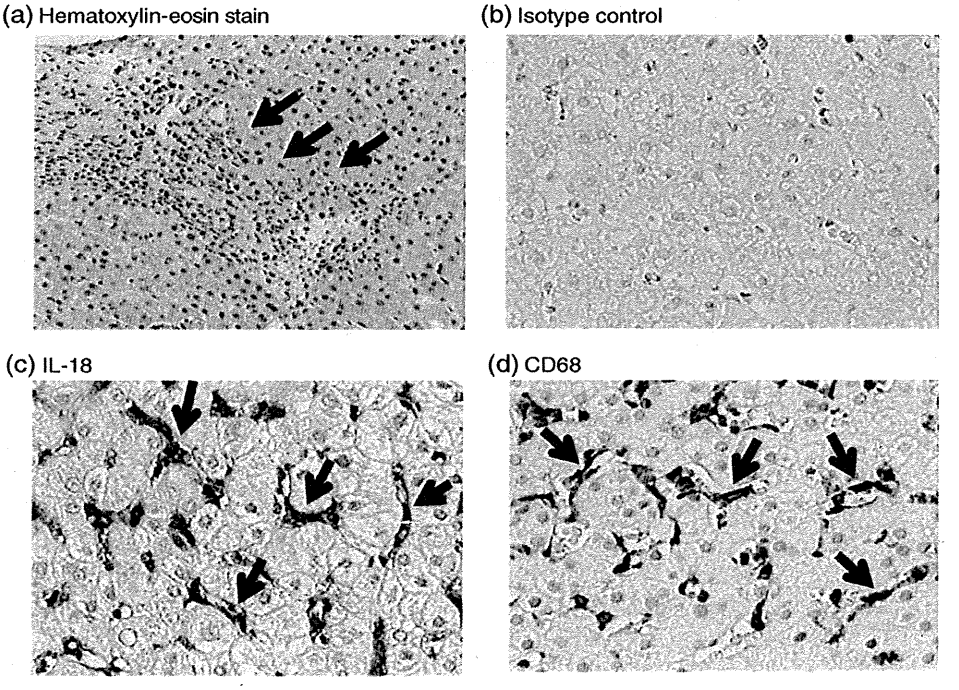

Fig. 4 Immunohistochemical analysis of liver tissue. After hematoxylin-eosin staining, examination showed interface hepatitis (*arrows*) and a heavy infiltrate of plasma cells in the portal tracts **(a)**. Isotype control is shown in **(b)**. CD68-positive cell infiltration and IL-18 expression are seen in the sinusoidal region (*arrows*) **(c, d)**

thyroiditis [18, 19]. We therefore speculate that both TPOAb and the previously mentioned cytokine signaling mechanisms may be causally related to our patient's hypothyroidism.

As discussed above, the pathogenesis of CMC and hypothyroidism caused by mutated *STAT1* can be explained by the combination of autoimmune disorders and cytokine dysregulation which have previously been reported. However, chronic active hepatitis is thought to be a rare complication, with unclear pathogenesis. We describe the pathogenesis of hepatitis caused by mutated *STAT1* as having both autoimmune and cytokine dysregulation mechanisms.

Hepatitis-associated autoantibodies may be positive in chronic active hepatitis caused by mutated *STAT1*. Our patient's chronic active hepatitis seems to be caused by a polyclonal increase in hepatitis-associated autoantibodies, such as ANA, ASMA, and anti-LKM-1 antibody. However, the pattern of these antibodies in this patient was thought to be atypical. Generally, ANA and ASMA are detected in type 1 autoimmune hepatitis, and anti-LKM-1 antibodies are detected in type 2 autoimmune hepatitis [20, 21]. The pathogenesis of hepatitis in this patient can therefore be explained by both autoimmune and other mechanisms. Our results also suggest that chronic active hepatitis caused by mutated *STAT1* may be associated with excessive IL-18 production. IL-18 was found to be a major factor in pathogen-associated molecular patterns induced hepatitis [22]. Liver biopsy showed CD68-positive cell infiltration, which is also seen in other disorders with cytokine dysregulation complicated by hepatitis such as Still's disease and mevalonate kinase deficiency [23]. It is well known that the autoantibodies are not associated with the pathogenesis of hepatitis in these two diseases. The hepatitis in our patient may be caused by excessive IL-18 accumulation due to recurrent mucocutaneous fungal infection. It is known that IL-18 binding protein induced by IFN-γ production mediates negative feedback of IL-18 production [24]. Decreased IFN-γ production by mutated *STAT1* therefore seems to cause increased IL-18 production.

At least one of the patients reported by van de Veerdonk et al. had chronic hepatitis, and that patient had a mutation of same amino acid residue (p.Arg274Trp) as our patient [8]. This may mean that a specific *STAT1* gene mutation (such as p.Arg274Trp or p.Arg274Gln) contributes to the pathogenesis of chronic hepatitis.

Conclusions

We present a rare case of AD-CMC with *STAT1* mutation complicated by both hypothyroidism and chronic active hepatitis. The pathogenesis of both CMC and hypothyroidism caused by mutated *STAT1* can be explained by the combination of autoimmune disorders and cytokine dysregulation. The pathogenesis of chronic active hepatitis in AD-CMC is still unclear. Our results suggest that hepatitis may be associated with the accumulation of IL-18. AD-CMC with *STAT1* mutation can be complicated by multiple immune disorders including APECED, with primary immune deficiency syndromes showing the phenotype of CMC.

Acknowledgments We thank Dr. K. Kubota, Dr. T. Yamamoto, and K. Kasahara for their advice and technical help. This work was supported by Grants-in-Aid for Scientific Research from the Ministry of Education, Science, and Culture of Japan and by Health and Labour Science Research Grants for Research on Intractable Diseases from the Ministry of Health, Labour and Welfare of Japan. The authors declare that they have no conflicts of interest.

References

1. Puel A, Cypowyj S, Bustamante J, Wright JF, Liu L, Lim HK, et al. Chronic mucocutaneous candidiasis in humans with inborn errors of interleukin-17 immunity. Science. 2011;332:65–8.
2. Nagamine K, Peterson P, Scott HS, Kudoh J, Minoshima S, Heino M, et al. Positional cloning of the APECED gene. Nat Genet. 1997;17:393–8.
3. Finnish-German AC. An autoimmune disease, APECED, caused by mutations in a novel gene featuring two PHD-type zinc-finger domains. Nat Genet. 1997;17:399–403.
4. Kisand K, Boe Wolff AS, Podkrajsek KT, Tserel L, Link M, Kisand KV, et al. Chronic mucocutaneous candidiasis in APECED or thymoma patients correlates with autoimmunity to Th17-associated cytokines. J Exp Med. 2010;207:299–308.
5. Holland SM, DeLeo FR, Elloumi HZ, Hsu AP, Uzel G, Brodsky N, et al. STAT3 mutations in the hyper-IgE syndrome. N Engl J Med. 2007;357:1608–19.
6. Zhang Q, Davis JC, Lamborn IT, Freeman AF, Jing H, Favreau AJ, et al. Combined immunodeficiency associated with DOCK8 mutations. N Engl J Med. 2009;361:2046–55.
7. Glocker EO, Hennigs A, Nabavi M, Schaffer AA, Woellner C, Salzer U, et al. A homozygous CARD9 mutation in a family with susceptibility to fungal infections. N Engl J Med. 2009;361:1727–35.
8. van de Veerdonk FL, Plantinga TS, Hoischen A, Smeekens SP, Joosten LA, Gilissen C, et al. STAT1 mutations in autosomal dominant chronic mucocutaneous candidiasis. N Engl J Med. 2011;365:54–61.
9. Liu L, Okada S, Kong XF, Kreins AY, Cypowyj S, Abhyankar A, et al. Gain-of-function human STAT1 mutations impair IL-17 immunity and underlie chronic mucocutaneous candidiasis. J Exp Med. 2011;208:1635–48.
10. Gough DJ, Levy DE, Johnstone RW, Clarke CJ. IFNgamma signaling-does it mean JAK-STAT? Cytokine Growth Factor Rev. 2008;19:383–94.
11. Dupuis S, Dargemont C, Fieschi C, Thomassin N, Rosenzweig S, Harris J, et al. Impairment of mycobacterial but not viral immunity by a germline human STAT1 mutation. Science. 2001;293:300–3.
12. Alvarez F, Berg PA, Bianchi FB, Bianchi L, Burroughs AK, Cancado EL, et al. International Autoimmune Hepatitis Group Report: review of criteria for diagnosis of autoimmune hepatitis. J Hepatol. 1999;31:929–38.
13. Yamauchi A, Iwata H, Ohnishi H, Teramoto T, Kondo N, Seishima M. Interleukin-17 expression in the urticarial rash of familial cold autoinflammatory syndrome: a case report. Br J Dermatol. 2010;163:1351–3.

14. Peterson P, Peltonen L. Autoimmune polyendocrinopathy syndrome type 1 (APS1) and AIRE gene: new views on molecular basis of autoimmunity. J Autoimmun. 2005;25(Suppl):49–55.
15. Smeekens SP, Plantinga TS, van de Veerdonk FL, Heinhuis B, Hoischen A, Joosten LA, et al. STAT1 hyperphosphorylation and defective IL12R/IL23R signaling underlie defective immunity in autosomal dominant chronic mucocutaneous candidiasis. PLoS One. 2011;6:e29248.
16. Park ES, Kim H, Suh JM, Park SJ, Kwon OY, Kim YK, et al. Thyrotropin induces SOCS-1 (suppressor of cytokine signaling-1) and SOCS-3 in FRTL-5 thyroid cells. Mol Endocrinol. 2000;14:440–8.
17. Amino N, Hidaka Y. Chronic (Hashimoto's) thyroiditis. In: DeGroot LJ, Jameson JL, editors. Endocrinology. 5th ed. Philadelphia: Elsevier Saunders; 2006. p. 2055–67.
18. Takasu N, Yamada T, Takasu M, Komiya I, Nagasawa Y, Asawa T, et al. Disappearance of thyrotropin-blocking antibodies and spontaneous recovery from hypothyroidism in autoimmune thyroiditis. N Engl J Med. 1992;326:513–8.
19. Takasu N, Matsushita M. Changes of TSH-Stimulation Blocking Antibody (TSBAb) and Thyroid Stimulating Antibody (TSAb) Over 10 Years in 34 TSBAb-Positive Patients with Hypothyroidism and in 98 TSAb-Positive Graves' Patients with Hyperthyroidism: Reevaluation of TSBAb and TSAb in TSH-Receptor-Antibody (TRAb)-Positive Patients. Journal of thyroid research. 2012;2012:182176. (Epub)
20. Manns MP, Czaja AJ, Gorham JD, Krawitt EL, Mieli-Vergani G, Vergani D, et al. Diagnosis and management of autoimmune hepatitis. Hepatology. 2010;51:2193–213.
21. Krawitt EL. Discrimination of autoimmune hepatitis: autoantibody typing and beyond. J Gastroenterol. 2011;46 Suppl 1:39–41.
22. Okamura H, Tsutsi H, Komatsu T, Yutsudo M, Hakura A, Tanimoto T, et al. Cloning of a new cytokine that induces IFN-gamma production by T cells. Nature. 1995;378:88–91.
23. Priori R, Barone F, Alessandri C, Colafrancesco S, McInnes IB, Pitzalis C, et al. Markedly increased IL-18 liver expression in adult-onset Still's disease-related hepatitis. Rheumatology (Oxford). 2011;50:776–80.
24. Muhl H, Kampfer H, Bosmann M, Frank S, Radeke H, Pfeilschifter J. Interferon-gamma mediates gene expression of IL-18 binding protein in nonleukocytic cells. Biochem Biophys Res Commun. 2000;267:960–3.

J Clin Immunol
DOI 10.1007/s10875-012-9805-x

ORIGINAL RESEARCH

In Vitro Analysis of the Functional Effects of an *NLRP3* G809S Variant with the co-Existence of *MEFV* Haplotype Variants in Atypical Autoinflammatory Syndrome

Kazuo Kubota · Hidenori Ohnishi · Takahide Teramoto · Eiko Matsui · Kana Murase · Hiroyuki Kanoh · Zenichiro Kato · Hideo Kaneko · Mariko Seishima · Naomi Kondo

Received: 24 July 2012 / Accepted: 17 September 2012

Abstract
Purpose Hereditary periodic fever syndromes have been considered monogenic diseases. However, some recent reports have described patients with co-existence of recurrent fever responsible genes. This study assessed whether a rare variant, found in Japanese children showing atypical autoinflammatory syndrome, located in the leucine-rich repeat domain of Nod-like receptor family, pyrin domain containing 3 (*NLRP3*) with co-existence of Mediterranean fever (*MEFV*) haplotype variants may contribute to a proinflammatory phenotype using a systematic approach.
Methods Cytokine production in serum or from peripheral blood monocytes was measured by ELISA. DNA sequence analysis of genes including *NLRP3*, *MEFV*, mevalonate kinase (*MVK*), and tumor necrosis factor receptor superfamily, member 1A (*TNFRSF1A*) were performed on patient samples. In vitro functional assays determined the effects of the NLRP3 variants and pyrin using NF-κB activation and speck formation assays.
Results A heterozygous genetic variant of *NLRP3*, G809S, was found in samples from both patients. Additionally the previously reported heterozygous *MEFV* variants (P369S-R408Q or E148Q-P369S-R408Q) were also detected in both patients. Serum IL-1ra and sTNFR1 levels increased in the attack phase of the disease in both patients. The production levels of IL-1β from monocytes isolated from both cases were elevated following LPS and IFN-γ stimulation. The *NLRP3* G809S variant demonstrated no increase of NF-κB activity following monosodium urate stimulation, whereas it significantly increased speck formation by interacting with apoptosis-associated speck-like protein with caspase recruitment domain.
Conclusions The phenotype of atypical autoinflammatory disease in patients could be modified by a synergistic effect with two other variants of autoinflammatory-associated genes.

Keywords NLRP3 · leucine-rich repeat domain · autoinflammatory disease · ASC

Abbreviations

ASC	Apoptosis-associated speck-like protein containing a CARD
CAPS	Cryopyrin-associated periodic syndrome
CINCA	Chronic infantile neurologic cutaneous, articular
FCAS	Familial cold-induced autoinflammatory syndrome
FMF	Familial Mediterranean fever
HEK	Human embryonic kidney
IL	Interleukin
MEFV	Mediterranean fever

K. Kubota · H. Ohnishi (✉) · T. Teramoto · E. Matsui · Z. Kato · N. Kondo
Department of Pediatrics, Graduate School of Medicine, Gifu University,
1-1 Yanagido,
Gifu 501-1194, Japan
e-mail: ohnishih@gifu-u.ac.jp

K. Murase · H. Kanoh · M. Seishima
Department of Dermatology, Graduate School of Medicine, Gifu University,
Gifu, Japan

H. Kaneko
Department of Clinical Research, Nagara Medical Center,
Gifu, Japan

Published online: 27 September 2012

MVK	Mevalonate kinase
MWS	Muckle–Wells syndrome
MSU	Monosodium urate
NBS	Nucleotide-binding site
NLRP3	Nod-like receptor family pyrin domain containing 3
NOMID	Neonatal-onset multisystem inflammatory disease
PAMPs	Pathogen-associated molecular patterns
PBMCs	Peripheral blood mononuclear cells
TNFRSF1A	Tumor necrosis factor receptor superfamily member 1A
TRAPS	Tumor necrosis factor receptor-associated periodic syndrome

Introduction

Autoinflammatory syndromes are characterized by systemic inflammation without the presence of antigen-specific T cells or high-titers of autoantibodies [1]. Many autoinflammatory syndromes are clinically characterized by recurrent or persistent features that include fever, elevation in the levels of acute-phase reactants, and organ-specific complications such as skin rashes and osteoarticular, serosal, neurologic, and ocular manifestations [2]. To date, well-known hereditary periodic fever syndromes are familial Mediterranean fever (FMF), hyperimmunoglobulinemia D with periodic fever syndrome, cryopyrin-associated periodic syndromes (CAPS), and tumor necrosis factor (TNF) receptor-associated periodic syndrome (TRAPS). These syndromes are discriminated by some characteristic phenotypes such as varying age of onset, duration of fever, development of cutaneous manifestations, and several other features.

CAPS include familial cold-induced autoinflammatory syndrome (FCAS), Muckle–Wells syndrome (MWS), and neonatal-onset multisystem inflammatory disease (NOMID), also known as chronic infantile neurologic, cutaneous, articular (CINCA) syndrome. FCAS exhibits cold-induced urticaria-like skin rash whereas MWS develops severe phenotypes, such as periodic fever, neural progressive hearing loss and renal amyloidosis. CINCA/NOMID syndrome shows additional more severe phenotypes, such as severe arthritis, patella overgrowth, aseptic meningitis, and mental retardation [3]. CAPS are caused by mutations in the Nod-like receptors (NLRs) family, pyrin domain containing 3 (*NLRP3*) gene, and more than 80 variants are associated with CAPS, in addition to over 50 variants of unclear significance that have been reported in the INFEVERS database (http://fmf.igh.cnrs.fr/ISSAID/infevers/) to date [4].

NLRs recognize microbial molecules such as pathogen-associated molecular patterns (PAMPs) or endogenous danger-associated molecular patterns, which trigger inflammation as well as Toll-like receptor immune responses. NLRP3 protein contains an N-terminal pyrin domain, a central nucleotide-binding site (NBS) domain, and C-terminal leucine-rich repeats (LRR) [5]. Most pathogenic mutations associated with autoinflammatory syndromes are located in exon 3 of *NLRP3*, which encodes the NBS domain. In addition, several mutations outside exon 3 on the LRR domain of *NLRP3*, such as G755R, G755A, and Y859C have been found in patients with CINCA syndrome or atypical autoinflammatory disorders [6–8].

This study reports two cases of Japanese children who presented with atypical periodic fever episodes and who had the variants in the LRR domain of *NLRP3* with co-existence of Mediterranean fever (*MEFV*) haplotype variants. The patients showed periodic prolonged fever and erythema, but lacked symptoms typical of CAPS, FMF, and other common autoinflammatory syndromes. By genetic analysis and functional assays of these variants, the data from this study suggest that the phenotype of atypical autoinflammatory disease in patients could be modified by a synergistic effect with other autoinflammatory-associated genes.

Methods

Subjects

Case 1

The first case was a 9-year-old girl who had experienced recurrent fever episodes approximately three times a year for 6 years from onset at 3 years of age. Although she underwent a tonsillectomy at the age of 5, she still experienced recurrent fever episodes. She presented with mild abdominal pain without signs of peritoneal irritation, peritonitis or pleuritis as typically observed in FMF. High serum C-reactive protein (CRP) levels were observed in the attack phase. She presented with pigmented macules with erythema, which persisted for 6 months, and bilateral petechiae on her legs and dorsa of feet (Fig. 1a). Histological examination of the skin lesion revealed perivascular infiltrate with mononuclear cells in the upper and middle dermis, but vasculitis was not observed (Fig. 1b). Direct immunofluorescence analysis revealed deposits of complement component 3 (C3) at the capillary walls in the upper to middle dermis, but not the presence of immunoglobulin (Ig)A or IgM (Fig. 1c). Rheumatoid factor and autoantibodies were not detected. Colchicine treatment (0.5 mg per day) was effective in treating the erythema and alleviating fever with elevating CRP. Both parents had experienced lasting recurrent fever episodes during their childhood although it was likely that their symptoms were not so severe. The fever episodes of parents resolved spontaneously without specific

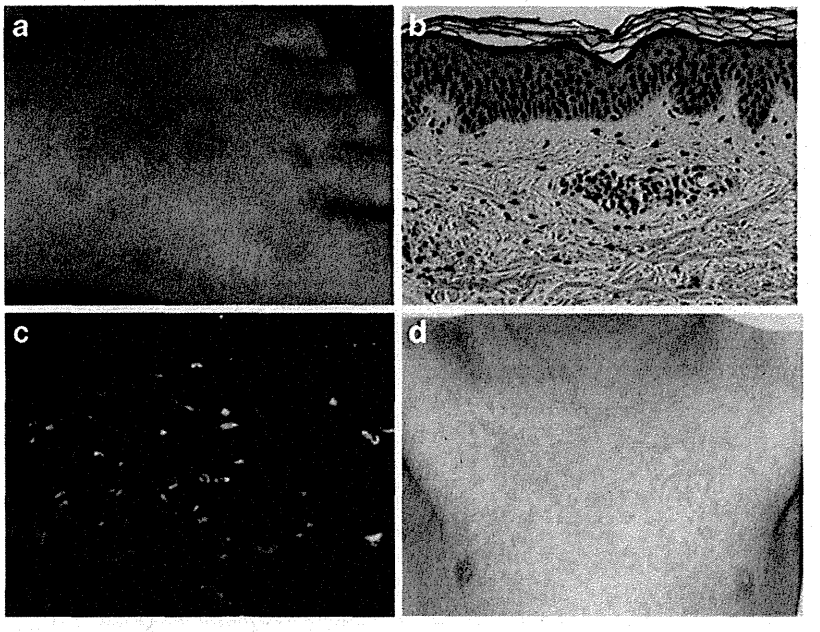

Fig. 1 Presence of skin rash in patients with atypical autoinflammatory syndrome. **a** The clinical appearance of rash on the dorsum of foot in case 1. **b** The histopathological examination of a skin biopsy specimen (hematoxylin and eosin stain, original magnification × 200). Perivascular infiltrate with mononuclear cells was observed in the upper and middle dermis. **c** Direct immunofluorescence demonstrates C3 deposits in the capillary walls (original magnification × 50). **d** The clinical appearance of the skin rash on the breast in case 2

medications such as colchicines and corticosteroids or tonsillectomy when they were about 10 years old. However, they do not remember their childhood in detail as it was over 30 years ago. Their episodes may represent autoinflammatory disease.

Case 2

The second case involved a 4-year-old boy, presenting with recurrent episodes of fever of various duration from a few days to weeks, with or without mild liver dysfunction and multiple erythema without skin itch. The frequency of episodes was at least twice a year. The skin erythema was observed during the fever episodes at 18 months old and at 4 years old (Fig. 1d). The cervical lymphadenopathy and diarrhea were observed in almost all of the fever attack episodes. Although fever duration was 1 week, it resolved immediately following oral administration of 1 mg/kg prednisolone. Rheumatoid factor and autoantibodies were not detected. His parents had no symptoms like periodic fever syndromes or rheumatic diseases. The fever did not recur for a few months after the cessation of oral prednisolone treatment. From 3 years old, colchicine treatment was started because of recurrent fever attacks. However, currently this treatment is not effective.

The genotypes and the clinical profiles of these cases are summarized in Table I. This study was performed according to the Helsinki Declaration. All subjects provided informed consent to participate in the study.

DNA Sequencing

Genomic DNA was extracted from leukocytes using SepaGene (EIDIA, Tokyo, Japan). DNA fragments of the *NLRP3*, *MEFV*, mevalonate kinase (*MVK*), and TNF receptor superfamily, member 1A (*TNFRSF1A*) genes were amplified by polymerase chain reaction (PCR), and analyzed using big dye terminator bidirectional sequencing (Applied Biosystems, Foster City, CA, USA).

Table I Genotype and clinical profiles of cases

	Case 1	Case 2
Initial diagnosis	FMF	TRAPS
Gender	Female	Male
Clinical features		
Age at onset of attacks	3 years	6 months
Duration of episodes	3–5 days	>1 week
Fever	Yes	Yes
Abdominal signs	Yes	Yes
Arthralgia	No	No
Lymphatic signs	No	Yes
Cutaneous manifestations	persistence of rash (pigmented erythema with petechiae)	Two episodes of rash
Hearing loss	No	No
Neurologic signs	No	No
Proteinuria	No	No
Laboratory findings		
WBC (/μl)	11,800	14,620
CRP (mg/dl)	10.1	3.1
ESR (mm/h)	45	32
NLRP3 Genotype	G809S	G809S
MEFV Genotype	P369S, R408Q	E148Q, P369S, R408Q

CRP the serum C-reactive protein level. *WBC* white blood cells. *ESR* erythrocytes sedimentation rate. Laboratory findings were the data in the attack phase

Genotyping

Allelic frequency of NLRP3 G809S (rs141389711) was investigated on a Step One Real-Time PCR System using Custom TaqMan SNP Genotyping assays (Applied Biosystems) in 421 healthy subjects. Further, genotype was confirmed by direct sequence analysis.

Cell Culture

Peripheral blood mononuclear cells (PBMCs) were isolated from heparinized blood of control donors and from patients by gradient centrifugation using Ficoll-Paque (GE Healthcare, Uppsala, Sweden). The CD14-positive cells were cultured in medium consisting of RPMI 1640 supplemented with 10 % heat-inactivated fetal calf serum (FCS), L-glutamine (2 mmol/l), penicillin (100 U/ml), and streptomycin (100 μg/ml). Human embryonic kidney (HEK) 293 T cells and HEK293-ASC cells were cultured in high glucose Dulbecco's modified Eagle's medium (Invitrogen, Carlsbad, CA, USA) supplemented with 10 % heat-inactivated FCS (Sigma-Aldrich, St. Louis, MO, USA), penicillin (100 U/mL), and streptomycin (100 μg/mL).

Analysis of Serum Cytokine Levels by Enzyme-Linked Immunosorbent Assay (ELISA)

Serum samples of patients and controls were stored at −80 °C until assayed. TNF-α concentrations were measured with an Immunoassay Kit (BioSource International, Carlsbad, CA, USA) with a detection limit of 1.7 pg/ml. Similarly, interleukin (IL)-6 and IL-1β concentrations were measured by immunoassay Kit (BioSource) with detection limits of 1.7 pg/ml and 1.0 pg/ml, respectively. IL-1ra and sTNFR1 concentrations were measured by ELISA (R&D Systems) with detection limits of 6.26 pg/ml and 0.77 pg/ml, respectively. IL-18 was assayed by ELISA (MBL, Nagoya, Japan), with a detection limit of 25.6 pg/ml. We defined serum cytokine levels of more than the mean + 2 SD as increasing. Values below the detection limit are shown as not detected.

IL-1β Production from Monocytes

CD14-positive cells were purified from PBMCs using CD14 MACS MicroBeads and MACS magnetic columns according to the manufacturer's instructions (Miltenyi Biotec, Gladbach, Germany). The CD14 positive cells were seeded to a density of 3.0×10^5 per ml and cultured with the addition of 1.0 μg/mL LPS O127 (Sigma-Aldrich) and 20 μg/ml IFN-γ (R&D Systems, Minneapolis, MN, USA) for 24 h at 37 °C in a humidified atmosphere at 5 % CO_2 and pulsed with 5 mM ATP (Sigma-Aldrich) for 30 min before harvesting. The cell-culture supernatants were harvested, and stored at −80 °C until assayed. The IL-1β was measured with ELISA. The assay was performed at two different times. The statistical significance between control and each case in the IL-1β production was analyzed using Dunnett's multiple comparison test. *P*-value of <0.05 was considered statistically significant.

Vector Preparations

cDNA encoding *NLRP3* tagged at the C-terminus with a FLAG-epitope (NLRP3-FLAG) was cloned into plasmid pcDNA3.1+ (Invitrogen). NLRP3 mutants (D303N, G755R, G809S and Y859C) were generated using the GeneEditor *In vitro* Site-Directed Mutagenesis System (Promega, Madison, WI, USA). A cDNA encoding pyrin tagged at the C-terminus with an HA-epitope (pyrin-HA) was cloned into plasmid pcDNA3.1+. Pyrin variants (P369S+R408Q) were generated using the GeneEditor in vitro Site-Directed Mutagenesis System (Promega). The apoptosis-associated speck-like protein containing a CARD (ASC) variant 1 tagged at the C-terminus with a myc-epitope (ASC1-myc) construct was cloned into pcDNA3.1+. The NF-κB luciferase reporter vector (pGL4.32-luc2P/NF-kappaB-RE/Hygro) and the Renilla luciferase reporter vector (pGL4.74-hRluc/TK) were purchased from Promega.

NF-κB Reporter Gene Activity

HEK293T cells were transfected with 16 ng per well of pcDNA3.1+ control vector or pcDNA3.1+ NLRP3-FLAG (wild type or mutant) or pcDNA3.1+ pyrin-HA (wild type or mutant) in 96-well plates using Lipofectamine 2000 (Invitrogen) according to the manufacturer's instructions. The pcDNA3.1+ ASC1-myc, NF-κB luciferase reporter, and Renilla luciferase reporter were co-transfected. After transfection, cells were incubated for 24 h. Cells were stimulated with R837 at a concentration of 10 μg/ml (InvivoGen, San Diego, CA, USA) or monosodium urate (MSU) at 250 μg/ml (InvivoGen) for 8 h. Luciferase reporter activity was analyzed using the Dual-Luciferase Reporter Assay System (Promega). The statistical significance of differences in luciferase activity between wild-type and mutant gene activity in the NF-κB reporter assays was analyzed using Dunnett's multiple comparison test. A *P*-value of <0.05 was considered statistically significant.

Speck Quantification Assay

HEK293 cells were transfected with ASC-myc and positively selected using 1 mg/ml G418 for 4 weeks. HEK293-ASC cells (1×10^5) were co-transfected with 250 ng of each NLRP3 expression plasmid and pyrin expression plasmid using Lipofectamine LTX (Invitrogen) according to the manufacturer's instructions. After 24-h incubation, cells were fixed with 3.7 % paraformaldehyde in PBS for 10 min,

and washed with 10 mM glycine in PBS. Fixed cells were permeabilized using PBS containing 0.2 % Triton X-100 for 1 h at room temperature. Cells were then incubated with an anti-FLAG M2 monoclonal antibody (Sigma-Aldrich) and anti-myc antibody (Invitrogen). Primary antibody binding was detected by incubation with Alexa Fluor 488 goat anti-mouse IgG and Alexa Fluor 594 donkey anti-rabbit IgG (Invitrogen) secondary antibodies. Fixed cells were incubated with 4'-6-diamidino-2-phenylindole, a nuclear stain, and mounted using Vectashield Mounting Medium (Vector Laboratories Burlingame, CA, USA). The percentage of cells containing ASC specks in the cells expressing *NLRP3* was calculated by randomly selecting at least 10 fields. Differences were analyzed using Dunnett's multiple comparison test. A *P*-value of <0.05 was considered statistically significant.

Results

Detection of NLRP3 and MEFV Mutations in Two Patients with Autoinflammatory Syndrome

In case 1, a heterozygous c.2425G>A (p.Gly809Ser) on LRR in exon5 of *NLRP3* and heterozygous P369S-R408Q in exon3 of *MEFV* were identified (Table I). There are 17 individuals who have the allele of G809S in 421 healthy control subjects. The allele frequency of this variant was 0.02. There were no control subjects carrying P369S-R408Q in *MEFV* in addition to the G809S variant. Interestingly, the same *NLRP3* and *MEFV* haplotype variants were identified in the father of case 1. The heterozygous *MEFV* variant haplotype P369S-R408Q were also observed in the mother of case 1.

Case 2 expressed the same heterozygous *NLRP3* variant found in case 1. In addition, heterozygous E148Q-P369S-R408Q in exon2 and exon3 of *MEFV* were identified (Table I). The G809S variant of *NLRP3* was inherited from his asymptomatic father. His asymptomatic mother was positive for homozygous E148Q and heterozygous P369S-R408Q sequences.

MVK and *TNFRSF1A* mutations were not detected in either case.

The Cytokine Profile of Patients

Serum IL-1β, IL-6 and TNF-α levels were not detected in the sera of healthy control subjects. The mean concentration ± SD of serum IL-18 and IL-1ra in healthy control subjects were 169.2±85.7 pg/ml and 213.4±87.1 pg/ml, respectively [9]. The mean concentration ± SD of serum sTNFR1 in healthy control subjects was 1009±276.4 pg/ml. Figure 2a and b show the serum cytokine profiles from the patients. The serum cytokine concentrations were measured at two different points at least during fever and inter-ictal periods respectively, and average values were calculated. In both cases, serum IL-1β,

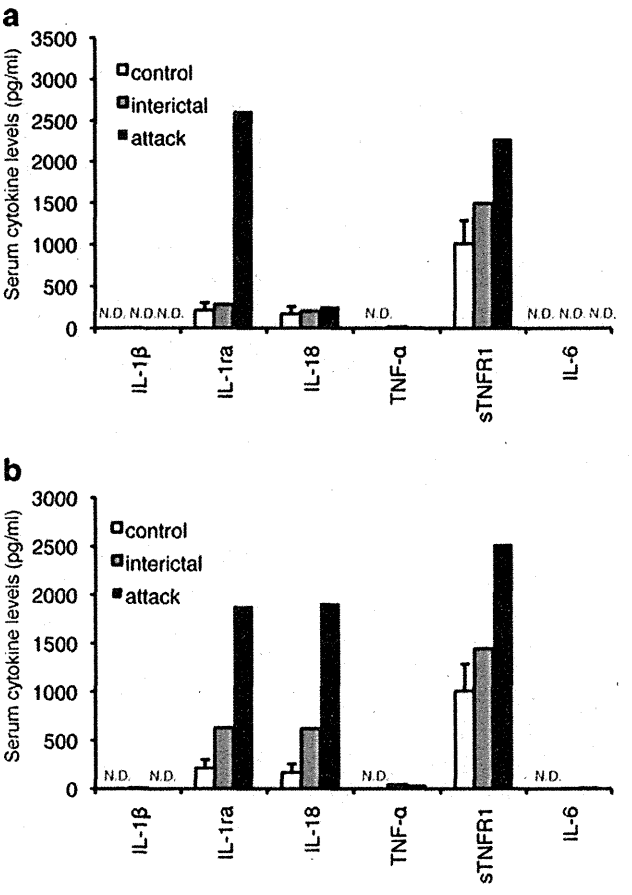

Fig. 2 Inflammatory cytokine levels from two cases during the inter-ictal phase and attack phase. **a** White bars indicate serum inflammatory cytokine levels of control. Grey bars indicate serum inflammatory cytokine levels of case 1 during the inter-ictal period. Black bars indicate serum inflammatory cytokine levels of case 1 during the attack phase. **b** White bars indicate serum inflammatory cytokine levels of control. Grey bars indicate serum inflammatory cytokine levels of case 2 during the inter-ictal period. Black bars indicate serum inflammatory cytokine levels of case 2 during the attack phase

TNF-α, and IL-6 did not increase during the fever episodes, whereas serum IL-1ra and sTNFR1 levels were increased. IL-18 levels during the fever episodes were increased in case 2, not in case 1. Interestingly, the serum IL-1ra and IL-18 levels from case 2 were elevated during the inter-ictal period.

Figure 3 shows the production of IL-1β from monocytes with LPS, IFN-γ and/or ATP stimulation. The mean concentration ± SD of IL-1β from monocytes of healthy control subjects ($n=5$) without stimulation were 5.54±4.40 pg/ml. The mean concentration ± SD of IL-1β from monocytes of healthy control subjects stimulated with 20 ng/ml IFN-γ or 1 μg/ml LPS were 7.74±9.81 pg/ml and 236.0±188.4 pg/ml, respectively. The mean concentration ± SD of IL-1β from monocytes of healthy control subjects stimulated with 1 μg/ml LPS added 5 mM ATP was 166.0±138.3 pg/ml. The mean concentration ± SD of IL-1β from monocytes of healthy

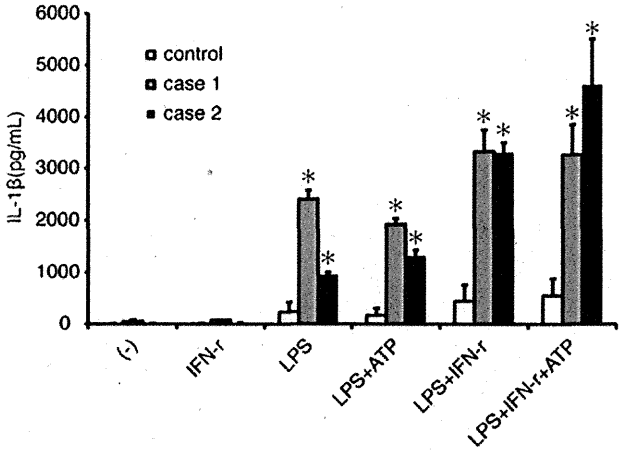

Fig. 3 IL-1β levels from monocytes in case 1 and 2. White bars indicate IL-1β levels in control. Grey bars indicate IL-1β levels in case 1. Black bars indicate IL-1β levels in case 2. IL-1β levels from monocytes from case 1 and 2 were significantly increased compared with controls (n=5). * P<0.05

control subjects stimulated with both 20 ng/ml IFN-γ and 1 μg/ml LPS were 441.3±316.5 pg/ml. The mean concentration ± SD of IL-1β from monocytes of healthy control subjects stimulated with both 20 ng/ml IFN-γ and 1 μg/ml LPS added 5 mM ATP was 549.2±327.3 pg/ml. In both cases, IL-1β secretion was increased compared with the healthy controls when the monocytes were stimulated with LPS and IFN-γ. Additionally, IL-1β from monocytes in case 2 stimulated with LPS and IFN-γ was increased in response to ATP. This was not observed for monocytes from case 1.

NF-κB Reporter Gene Activity of NLRP3 and Pyrin Variants

To assess the function of the *NLRP3* variant G809S on NF-κB signaling, we compared the G809S sequence with those of wild-type and three *NLRP3* mutations (D303N, G755R and Y859C). D303N, G755R, and Y859C were identified in CAPS patients [6, 10, 11] (Fig. 4). When ASC was co-expressed, D303N and G755R mutations increased NF-κB reporter gene activity. However, G809S and Y859C did not lead to significant activation of NF-κB. In the presence of R837, an *NLRP3* inflammasome activator, *NLRP3* D303N and G755R mutations showed enhanced NF-κB activation, whereas G809S and Y859C did not induce any increase in activity. Subsequently, the evaluation of G809S enhanced NF-κB activation in the presence of MSU was measured. MSU induced NF-κB activation of wild-type, D303N and G755R *NLRP3*. However, both G809S and Y859C mutations significantly inhibited NF-κB activation mediated by MSU.

To investigate the role of mutational effect of pyrin in the NF-κB signaling pathway, wild-type or variant pyrin (P369S+R408Q) was expressed in HEK293 cells and co-

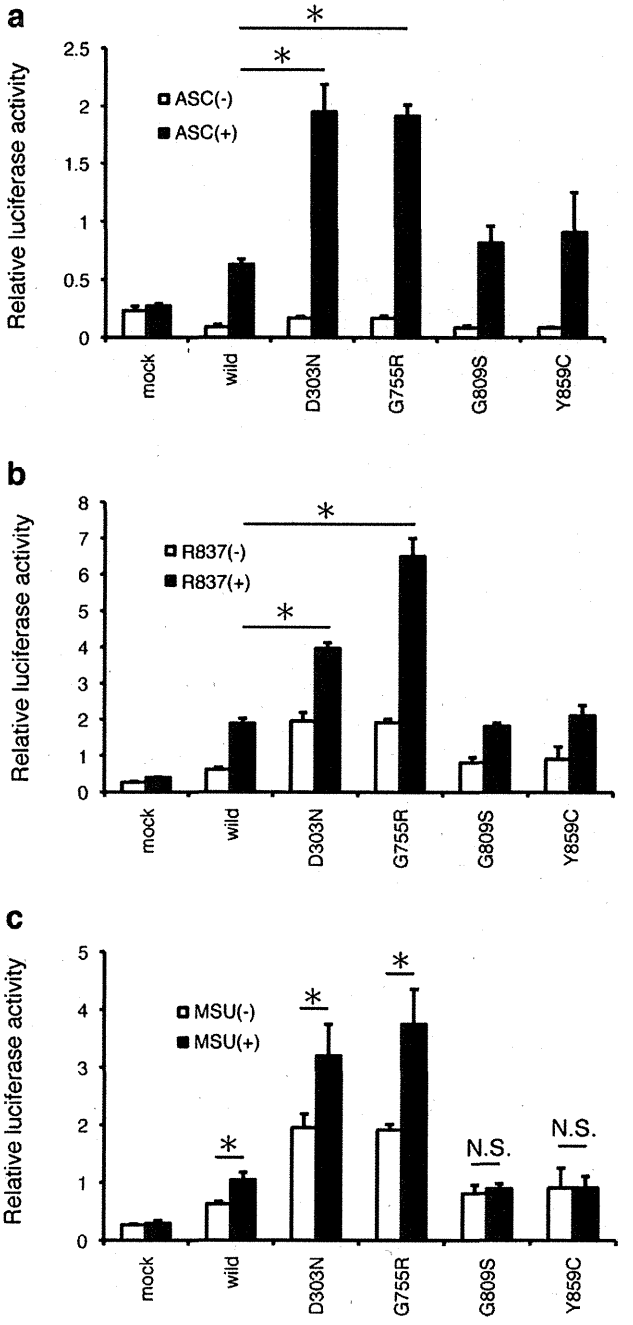

Fig. 4 NF-κB reporter gene activity of *NLRP3* mutants. Bars represent the mean ± SD of triplicate assays. **a** White bars indicate the NF-κB reporter gene activity of the *NLRP3* mutants without co-transfection of ASC. Black bars indicate activity with co-transfection of ASC. ASC-dependent NF-κB reporter gene activity was increased by mutants D303N and G755R. G809S and Y859C did not induce NF-κB reporter gene activity. **b** White bars indicate NF-κB reporter gene activity with co-transfection of ASC. Black bars indicate activity after stimulation with 10 μg/ml R837. **c** White bars indicate NF-κB reporter activity following co-transfection of ASC. Black bars indicate activity after stimulation with 250 μg/ml MSU. * P<0.05

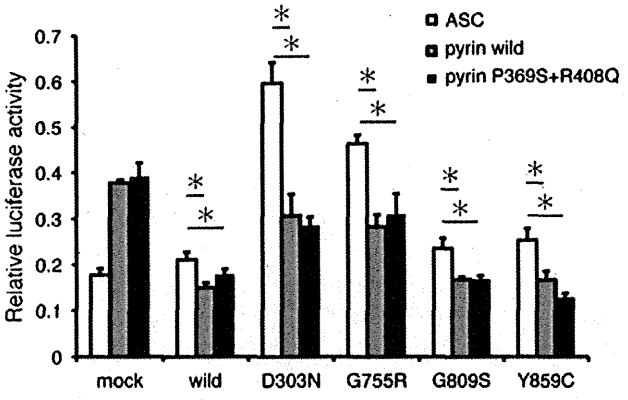

Fig. 5 Pyrin and *NLRP3* mutant-induced NF-κB reporter gene activity. Bars represent the mean ± SD of triplicate assays. White bars indicate NF-κB reporter gene activity with co-transfection of ASC. Grey bars indicate activity with co-transfection of ASC and wild-type pyrin. Black bars indicate activity with co-transfection of ASC and pyrin variant P369S+R408Q. * $P<0.05$

transfected with ASC (Fig. 5). Although both wild-type and variant pyrin inhibited NF-κB activation with co-transfection of wild-type or mutant NLRP3 protein, there was no significant difference in inhibitory capacity between the wild-type and variant pyrin.

Speck Quantification Assay

Previous studies have shown that *NLRP3* LRR variants have an increased ability to induce speck formation in the presence of ASC [6, 12]. To test the effect of G809S on *NLRP3*-ASC interactions and speck formation, wild-type, *NLRP3* variants or empty vectors and pyrin were transiently transfected with cells stably expressing ASC. Cells transfected with *NLRP3* wild-type displayed speck formation (mean ± SD, 36.7± 6.1 %). In comparison, the *NLRP3* D303N, G755R, G809S and Y859C mutants induced significantly higher numbers of speck formation (62.1±8.8 %, 72.6±4.8 %, 53.1±10.1 % and 48.8±13.2 % respectively, Fig. 6).

Discussion

The current study identified a G809S variant within the LRR domain of *NLRP3* with the co-existence of *MEFV* haplotype variants in two unrelated patients with atypical autoinflammatory syndrome. Although we recently reported a CINCA/NOMID patient with the compound heterozygous gene mutations E688K and G809S, it is unclear whether G809S is a pathogenic mutation [9]. To confirm a functional role for the G809S variant, its effect on the NF-κB signaling pathway was investigated in vitro. Although several variants of *NLRP3* show significant increases of ASC dependent NF-κB reporter gene activity in a previous report and as data presented here, no significant increase was observed owing to the *NLRP3* G809S variant in this assay. Kambe et al. demonstrated that the *NLRP3* G755R mutation located within the LRR domain could induce significant NF-κB activation in the presence of an *NLRP3* inflammasome activator, R837 [13]. Therefore,

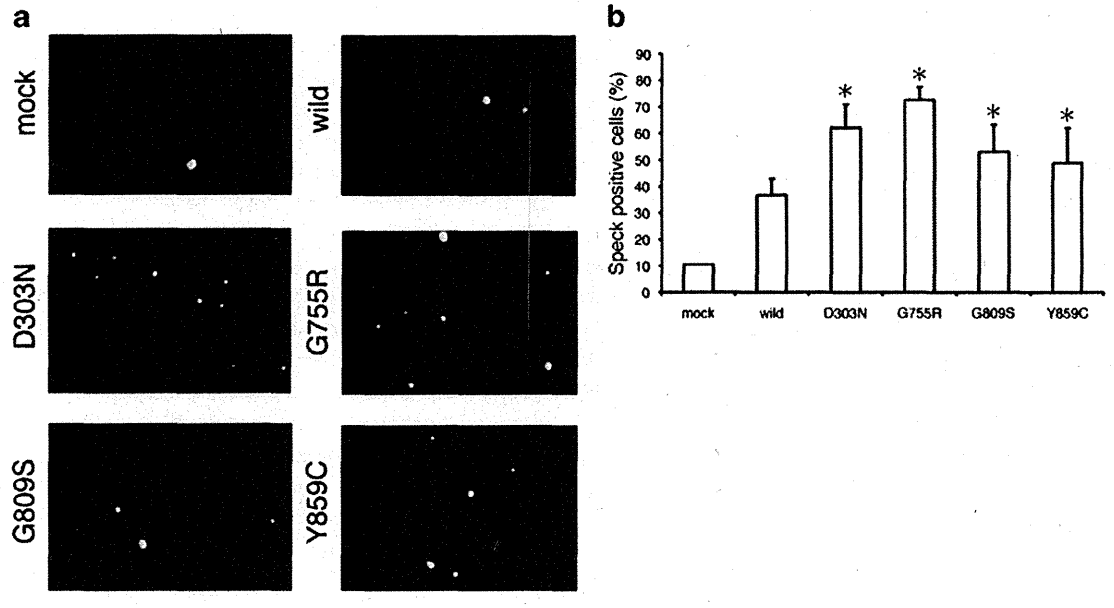

Fig. 6 Effect of the G809S variant on speck formation. Transfection of HEK293-ASC cells with 250 ng each of the *NLRP3* expression plasmids or an empty vector and pyrin expression plasmid was performed. Speck formation was assessed by immunofluorescence microscopy. **a** This panel shows examples of fields obtained by immunofluorescence microscopy. **b** The percentage of cells containing ASC-myc specks was calculated as the mean ± SD percentage of cells. * $P<0.05$